POLITECNICO DI TORINO

Collegio di Ingegneria Meccanica, Aerospaziale, dell'Autoveicolo e della Produzione

Corso di Laurea Magistrale
in Ingegneria Meccanica

Tesi di Laurea Magistrale

Effects of the process parameters on the dimensional and geometric quality of the components produced by the electron beam melting process

Relatori:

Prof. Luca Iuliano
Ing. Manuela Galati
Prof. Paolo Minetola

Candidato:

Salvatore Varveri

A.A. 2019/2020

Summary

INTRODUCTION

Electron beam melting (EBM) is a revolutionary technique of additive manufacturing (AM) process that permits to produce mass-customized parts from various metallic materials. The technique allows the production of parts with complex geometry starting from the powder that is selectively melted through an electron beam, layer-by-layer strategy [1]. Recently this technology has found a remarkable success especially in sectors where there is the need to produce pieces with very complex and high quality geometry, such as the biomedical and aerospace sector. Moreover, this manufacturing process has the interesting property of being able to manufacture parts in titanium alloy without incurring the problems of traditional production. This has brought considerable interest in science and industry about this process; however, in the literature there is not yet a systematic study on improving the quality of the product and on optimizing the process parameters, especially about titanium aluminides**,** a very interesting alloy due to its mechanical and thermal properties. These innovative materials have low density but excellent resistance and creep properties up to 750 ° C, as well as good resistance to burns and oxidation [2]. Hence, the interest in aerospace and biomedical as well as other sectors such as super cars where there is a need to use resistant but light pieces at the same time. This study discuss the optimization of EBM process parameters in the manufacture of titanium aluminides, with a focus on the contour strategy, which uses a technology known as MultiBeam. This strategy improves the quality of the product in terms of dimensional tolerances and defects such as porosity, solving some critical issues of EBM.

1. ELECTRON BEAM MELTING PROCESS

EBM is a processes of the additive manufacturing technology, which allows the manufacture of any complexity geometry layer by layer, without the necessary use of other tools or machines [3]. This AM process allows, using a high energy, the melting of metal powder. It is one of the few AM processes that allows the production of functional parts and not just prototypes. It is capable of working countless metals like such as stainless steel (17-4), tool steel (H13), Ni-based super alloys (625 and 718), Co-based super alloys (Stellite 21), low-expansion alloys (Invar), hard metals (NiWC), intermetallic compounds, aluminium, copper, beryllium and niobium [4]. However, as already mentioned, recently this process has found considerable progress concerning the production of titanium alloy parts. This process avoids the problems encountered in working this alloy with traditional technology, such as the high melting temperature, low fluidity and high reactivity with oxygen, making the process complicated and expensive [2].

1.1 Operating principle

The EBM working in vacuum environment which avoids the problems mentioned, with a high-energy source given by an electron beam. An effective description of the working principle is described in the article published by L. Iuliano and M. Galati [3], comparing the EBM system to a welding machine, with an operating principle similar to an electron microscope. The technology developed by Arcam [5], consists of two main parts: the electron beam unit and the build chamber. The highest part of the electron beam unit contains the electron generation part, which is subsequently formed and deflected by magnetic lenses in the lower part of the unit. The electron

generation part consists of a heated filament (cathode), which is heated to high temperature and emits electrons, with a potential between cathode and anode usually of 60 V and an acceleration of the electrons from 0.1 to 0.4 times the speed of light [3]. The Electron Beam unit is fixed and the beam is controlled with three magnetic lenses, without the use of mechanical parts. The first magnetic field (astigmatic lenses) is responsible for beam shape, and the second field (focus lenses) controls the size of the beam. The last magnetic field (deflection lenses) deflects the focused beam to the desired position on the building table [3], [5]. The entire process takes place in a vacuum, through a turbomolecular pump [3], at a pressure of about 10^{-3}Pa , to avoid impurities such as oxides and nitrides [5]. Moreover, there is the addition of helium, which acting as an inert gas, ensures thermal stability and prevents the accumulation of electric charges in the powder. The build chamber can be described in three main parts: the steel build tank, the powder feeder and the raking system. The steel build tank contains the start plate, constituting the XY plane of construction, while the Z axis perpendicular to the plane, it is the axis where the plate moves by a height equal to the layer executed. In the upper part of the chamber in the right and left corners, there are the powder feeders, which contain the powder that will be distributed into the build plane through the rake system, which has the purpose of collecting the powder on both sides and to distribute it evenly on the plane. The rake system other to distribute the powder, controls the amount of powder to be distributed in order to ensure a uniform layer, through a particular sensor that monitors the amount of powder distributed, because an uneven layer causes problems such as lack of fusion and the pushing phenomenon [6]. Typically the layer thickness amounts between 0.050 mm and 0.200 mm, depending on the powder material [7]. The spherical powder, with a size between 45 and 100 microns to ensures safe handling, is produced through the gas atomization method [8] or by means of a plasma rotating electrode process. Figure 1 shows schematic drawing of an electron beam melting system.

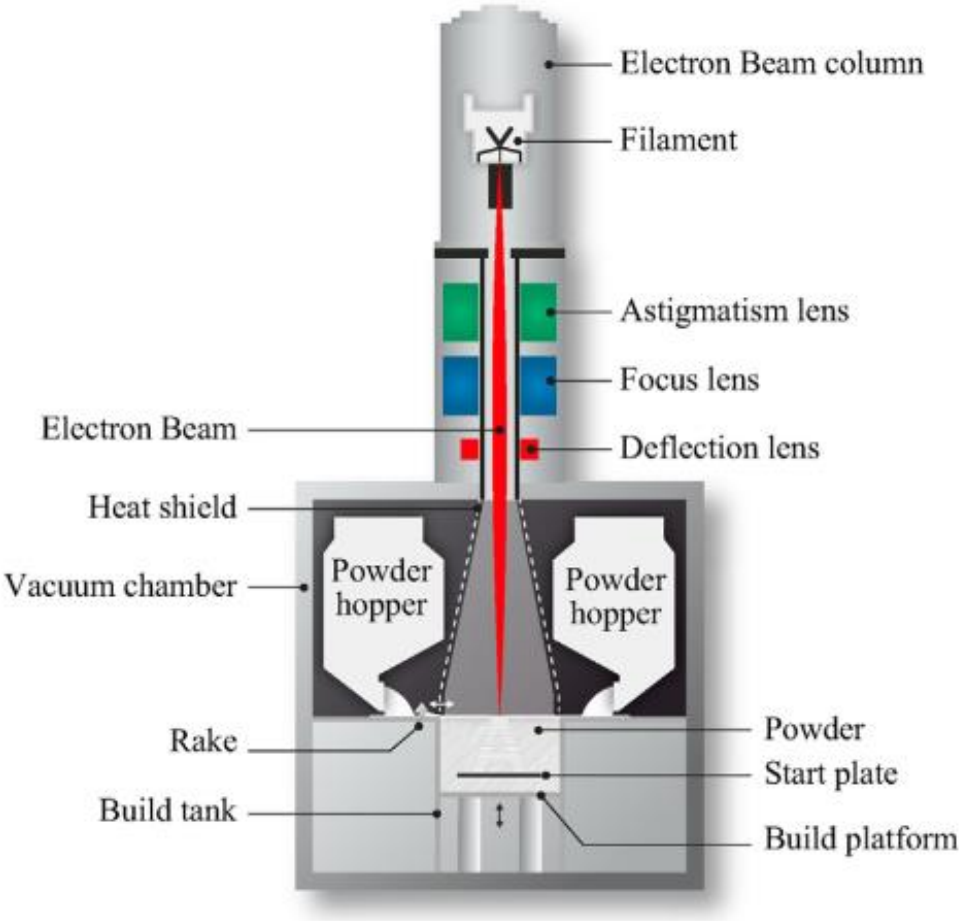

Figura 1 Component of EBM Arcam machine.

Like most AM processes, EBM process use slice data through a file format called SLC. The file defines the geometry of each single 2D section, and the distance between two slices. The building process begins with the heating of the start plate, at an appropriate temperature, according to the powder material that has to be melted [9]. When the plate, controlled by a thermocouple, has reached the desired temperature, the real construction process begins.

1.2 The construction process.

The main stages of the construction process are:

- Preheating and sintering the entire build region. It occurs through a series of defocused beam passages at high power and high speed (eg 15,000 mm / s and 30 mA [3]). This is to minimize the thermal gradient and therefore the internal stresses within the part, and ensures the electrical conductivity, for the incident electrons before the fusion cycle. It also avoids the problem of pushing phenomenon. This phenomenon appears as an explosion, caused by the intersection of the electron beam and the powder (figure 2). Generation occurs for various reasons, such as the presence of residual water, a negative electrostatic charge of the powder particles and the moment transferred by the electrons, much stronger than the cohesion of the powder. Preheating can reduce these causes, as with sintering, the total weight and conductivity of the powder increases, managing to counteract this force [3]. Preheating usually consists of two phases: Preheating I which scans the entire plane and Preheating II which scans the areas to be melted enlarged by 5 mm from the edges of the section [10].

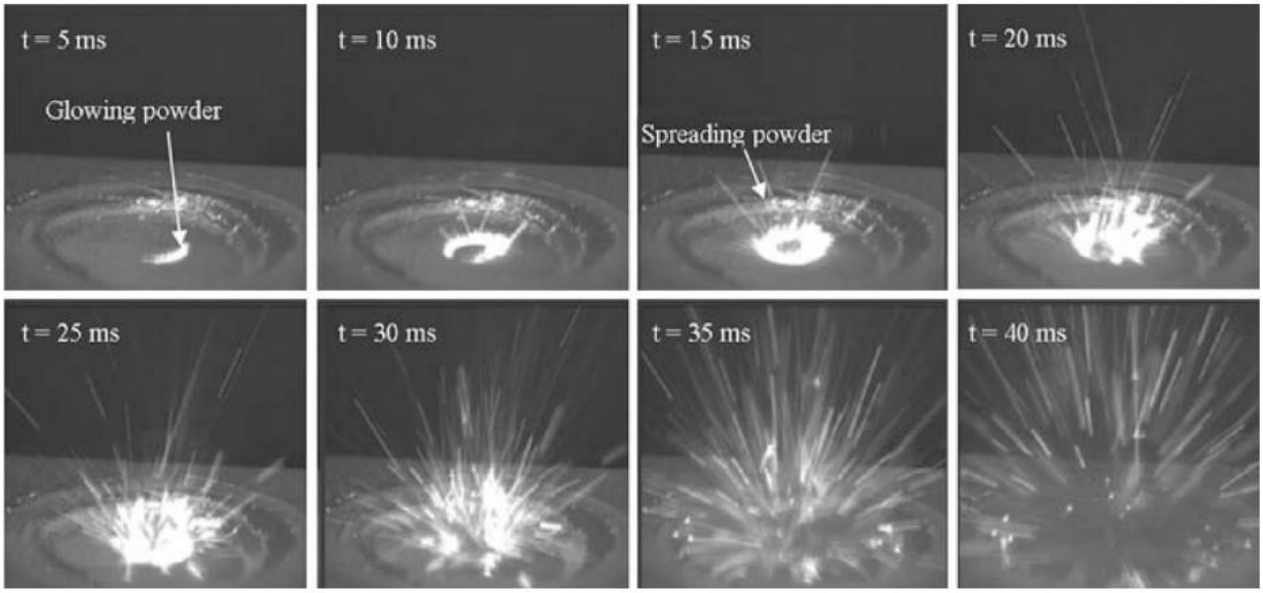

Figure 2 Pushing phenomenon [11]

- Melting of the powder, where the power and the scan speed are decreased, in accordance with the part to be produced and the material [3].
- A possible post heating.
- Successively the build table is lowered by a height equal to the thickness of the defined layer, and the hoppers supply the powder which will then be raked for the formation of the next layer. the process is repeated until the job is complete
- When the piece is completed there is a slow cooling, assisted by the increase of helium pressure.
- At the end of the process, the piece is complete and is immersed in an agglomeration of unmelted powder. This agglomerate is called breakaway powder [12] and is removed by sandblasting, using the same powder used in the EBM process, to avoid diffusion problems.
- Since the whole process takes place in a vacuum, the powder is not chemically altered and is entirely recycled for the construction of new pieces [3].

2 PROCESS PARAMETERS

As already mentioned in the previous paragraphs, EBM technology offers countless advantages compared to conventional processes. However controlling the process parameters in order to optimize the construction of the product in terms of geometric deviation and defects such as porosity is not simple, since the phenomena that arise during the fusion are multiple and difficult to control simultaneously.

2.1 Effect of process parameters

It is evident that alterations in the preheating cycle and in the melting scan can have significant variations in the cooling rate and therefore in the microstructure, as well as in the sintering and melting efficiency. For example, if faster scans are performed, keeping the beam current constant, there is a reduction in the energy density of the focal point, while if the beam current is increased, with constant scan speed, the opposite effect is obtained. In theory, it is possible to vary the porosity of the entire build with the selective variation of the beam scan [12]. Figure 3 shows an example of optimization of these parameters, and with the related variation of the material's characteristic.

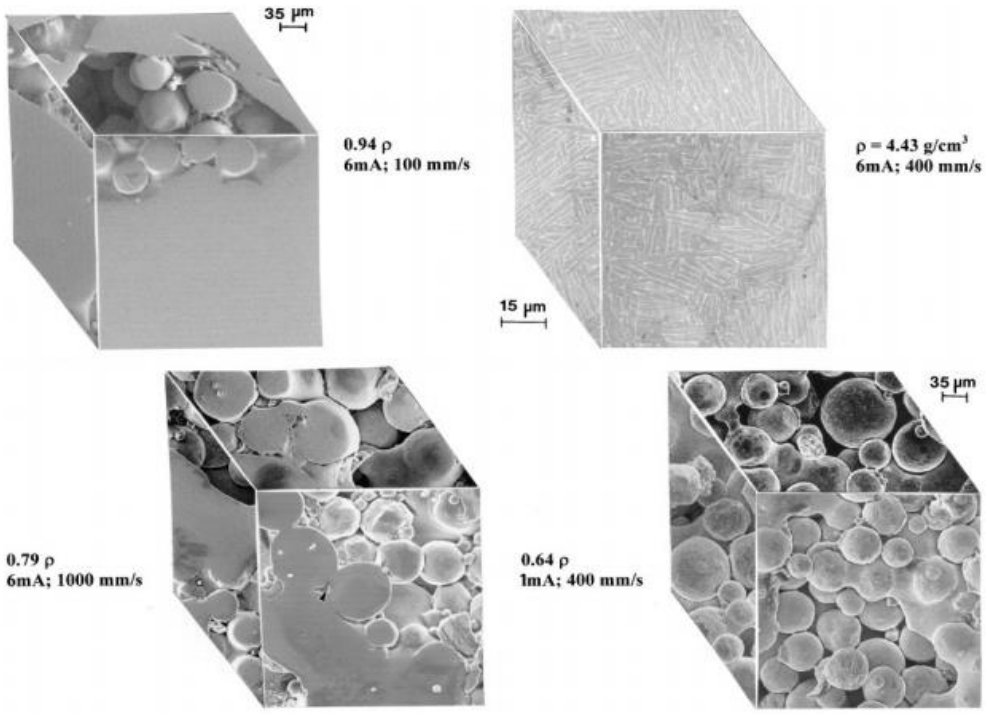

Figure 3 density variation of Ti – 6Al – 4V alloy, as the melting parameters change [12]

Other parameters in addition to the scanning and current speed, have a key role in various aspects; the table 1 shows the main features that influences the characteristics of the piece produced [3]. Table 1, which is a summary of experimental studies, shows how we can improve some characteristics of the product by selecting the right set of parameters, using an experimental trial and error approach, as will be examined in this work, for titanium aluminides. Obviously, the results are valid only for the range of values examined in the study, since there are process deficiencies, improvements are obtained by calibrating the parameters for the appropriate material, and the results are valid for the interval considered.

	How to improve	Reducing	Increasing
Feature Quality	Surface roughness	• Layer thickness • Focus offset • Beam current • Line offset • Line energy	• Scan Speed • Focus offset • Particle size
	Porosity and unmelted region	• Line offset • Scan speed • Argon trapping in the manufactured part can be removed through the HIP process • Focus offset	• Line energy
	Delamination	• Focus offset • unidirectional scanning raster	• Energy density

Table 1 main sets of parameters to improve product quality[3].

2.2 The main parameters

For clarity, and to understand the topics developed in the following paragraphs, the main EBM parameters are listed:

- acceleration voltage, usually kept constant at 60 KV, so that the power is directly proportional to the current [10].
- The beam current, during the hatching it is not automatically provided by the operator, but is calculated by the EBM control software and varies linearly with the length of the hatch line, so that smaller melting lengths have less current[10].
- focus offset, is the additional current that flows through the respective electromagnetic coil and can be translated into a focal plane offset from its zero position. The optimal value must be determined individually for each system. The beam current and focus offset jointly control the size of the spot, a change in the focus offset in the range of ± 10 mA results in a change in the beam diameter of approximately 0.05 mm [13].
- layer thickness
- Scan speed, which can be controlled directly or through a speed function, which inserted as a process parameter controls the beam speed. The scanning speed is a relevant parameter, a "speed function" is used to preserve a constant depth of the melting pool while maintaining an approximately constant ratio of P/v (proportional to I/v)[10]. It affects the size of the fusion pool but also the porosity, and the granular structure.
- The scanning process, as previously described: preheating, melting, and post heating. Which consists of the various steps that the beam performs during the construction of the product.

- The scanning mode, It consists in the path that the beam must perform to melting the single layer. There are various strategies to melt the layer, an example is what Arcam suggests as standard, which consists of hatching and 3 contour. Hatching is the internal melting of the section, which usually occurs with a "snake" path with parallel lines that follow one another, and the direction between adjacent layers was rotated 90°[14], as can be seen from Fig.5. A main parameter of hatching is the line offset, which determines the distance between two lines. The contour is the melting of the external part of the section, it provides an interface between the actual build and the surrounding powder. A fusion of the profile also offers the opportunity to have a good surface structure figure 4 illustrates these strategies.

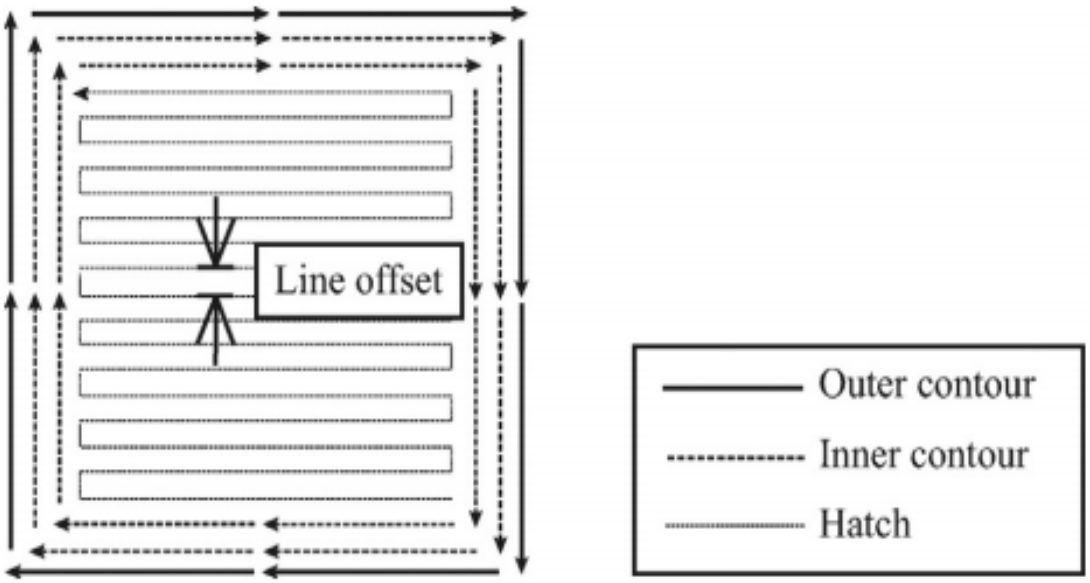

Figure 4 scanning mode [10].

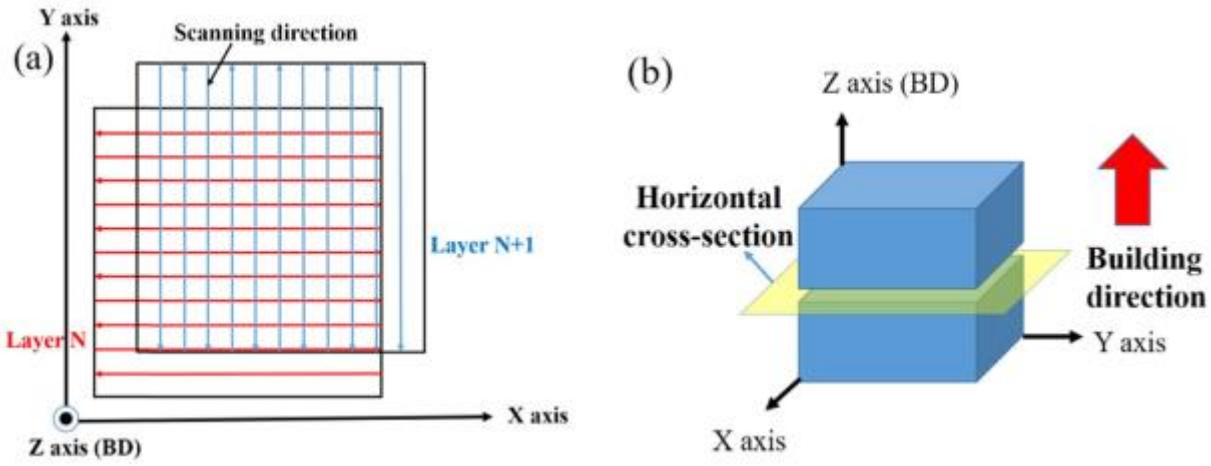

Figure 5 The scanning strategy of the SEBM process. The arrow shows the scanning direction of the electron beam and 90 ° is rotated between the adjacent layers N and N + 1.[14]

For the execution of the Contour, a particular technique can be used, which will be discussed in the following paragraphs, called MultiBeam. This strategy, maintains active different melt pools simultaneously, moving the beam quickly. In addition to the discussed parameters, which are controlled directly from the machine using the software, there are two other summary parameters, a combination of the process parameters mentioned, which are very important for following particular aspects such as the porosity and the microstructure of the job. The first is called energy density (E_v), which is expressed as eq. (1)

$$E_v = \frac{U \cdot I}{v \cdot d \cdot h} \quad (j \cdot mm^{-3}) \tag{1}$$

where: U,I,v,d and h are the voltage(V) beam Current (A), beam velocity (mm·s-1), line offset (mm) and layer thickness (mm),respectively. It defines the local heat input for unit volume, respect to the simultaneous variation of the beam speed, power and line offset [10].

The second parameter is called line energy (E_L), eq.(2)

$$E_L = \frac{U \cdot I}{v} \qquad (j \cdot mm^{-1}) \tag{2}$$

It defines the heat input for scan speed [15].

3 MICROSTRUCTURE AND MECHANICAL PROPERTIES OF γTIAL ALLOYS AS A FUNCTION OF THE PROCESS PARAMETERS.

As previously mentioned, TiAl alloys have attracted significant interests in the aerospace industry in recent decades due to their low density, specific resistance to high temperatures and excellent resistance to oxidation and corrosion. However, the low deformability at room temperature and the fragility limit their further application. But thanks to AM technology there is the possibility to process these alloys, an example of which is the electron beam melting and selective laser fusion (SLM). These technologies are capable of producing pieces with higher mechanical properties than traditional production technologies such as casting and forging, due to the small melting pool and the rapid cooling rate. In addition, the EBM, with respect to the SLM, has the advantage of being able to achieve preheating temperatures around 1100 °C, which is essential for the fusion of TiAl alloys, while the SLM process is performed with temperature lower than 300 C°[16]. Thanks to high EBM preheating temperature, it is possible to avoid the generation of cracks by releasing the thermal stress accumulated during the process [14]. In addition, the EBM working under vacuum, this advantage reduces the problem of contamination and porosity, lowing

densities of greater than 99.8% to be achieved [10]. Hence the growing interest for EBM in the manufacture of TiAl alloys.

3.1 Scan speed

The process parameters have a significant influence on the microstructure and mechanical properties of the products. With the variation of the scanning speed there is a considerable difference in the microstructure of the TiAl alloys, some examples are the studies done by Yuying Chen et al. [14], which reports the results obtained from different Ti-47Al-2Cr-2Nb samples by varying the scanning speed. Figure 6 shows the microstructure obtained by SEM analysis of 4 samples obtained with speeds 1500 mm/s, 1800 mm/s, 2100 mm/s and 2400 mm/s. Fig. 6(a) illustrates the microstructure of sample 1 with a scanning speed of 1500 mm/s, composed of alternating strips γ (gray) and and β_2 (glossy). In addition, in the lamellar colonies there is the presence of some equiaxial γ granules, while the α_2 phase cannot be distinguished. For the S2 sample with 1800 mm/s (fig. 6b), the width of γ lath is less than S1, but the rest of the structure remains unchanged, consisting of the strips γ and lamellae β_2, and the presence of phases γ equixate and β_2 blocks that are distributed on the edges of the grain. With increasing speed up to 2100 (sample S3) there is a significant difference in the microstructure which transforms into a duplex structure. It consists of fine lamellar colonies and equiaxed γ grains, with phase β_2 dispersion along the boundaries of the colonies (fig.6c). With the increase of the speed up to 2400 mm / s (sample S4), there is no significant variation, the structure is similar to sample S3 but the microstructure of sample S4 shows a much finer lamellar spacing [14].

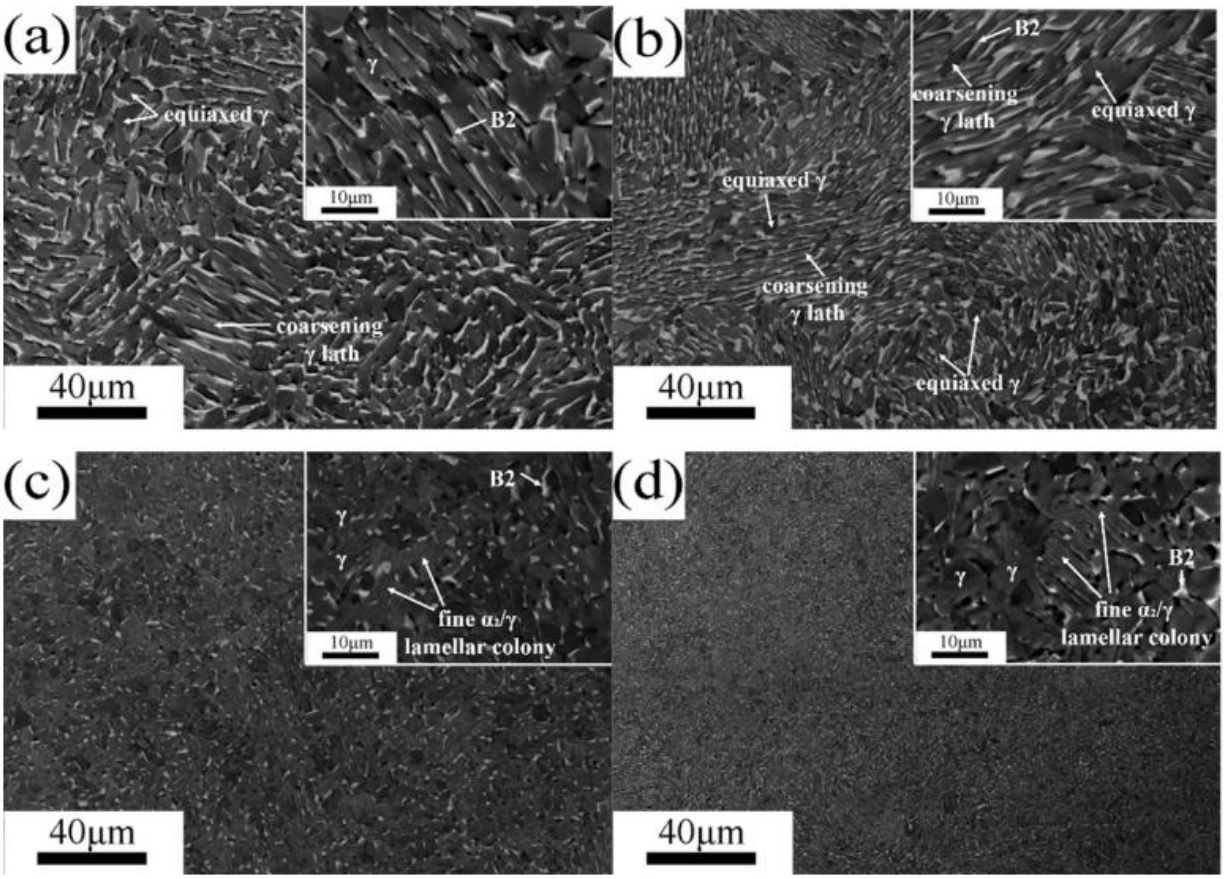

Figure 6 Image of the microstructure obtained by SEM analysis of the Ti-47Al-2Cr-2Nb samples obtained at speed (a) 1500 mm/s, (b) 1800 mm/s, (c) 2100 mm/s and (d) 2400 mm/s [14].

With TEM analysis it was possible to further study the microstructure of the samples, looking for phenomena that the SEM analysis was unable to show as for example the $\boldsymbol{\alpha_2}$ lamella which cannot be observed or detected by SEM observation due to the low width of the lamella [14]. Figure 7 shows the results obtained. Figures 7a and b show a microstructure formed by equilaxed and coarse laths γ and a dispersing blocky $\boldsymbol{\beta_2}$ phase at the boundaries of the colonies, with a scarce observation of lamellar colonies (sample S1). Fig. 7c and d (sample S2) show the phases γ and $\boldsymbol{\beta_2}$ equiaxed, but also highlight a remarkably decomposed lamella $\boldsymbol{\alpha_2}$, with a precipitation of $\boldsymbol{\beta_2}$ phase at the disconnection point of $\boldsymbol{\alpha_2}$ lamella. In sample S3 (figure 7e) the microstructure also shows the decomposition of $\boldsymbol{\alpha_2}$ lamellae, but the degree of decomposition is less than the sample S2. Finally, the sample s4 (figure 7f), in addition to showing a much finer

lamellar spacing, has a weaker decomposition of the lamella $\boldsymbol{\alpha_2}$ compared to the sample S3.

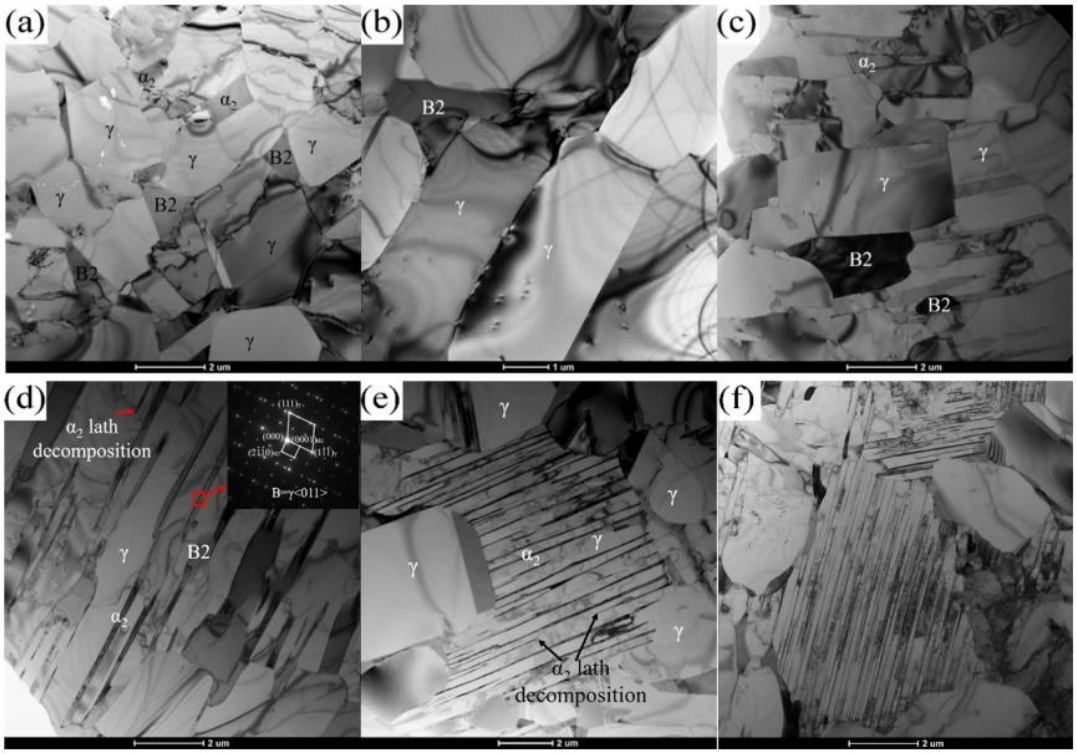

Figure 7 TEM images analysis of the Ti-47Al-2Cr-2Nb samples obtained at speed (a,b) 1500 mm/s, (c,d) 1800 mm/s, (e) 2100 mm/s and (f) 2400 mm/s [15]

Moreover, the images obtained by EBSD are shown (figure 8), which displays the variation in phase composition as the scanning speed change. It can obviously be observed that with increasing speed the percentage of phase α_2 and β_2 decreases while the content of phase γ increases. The respective percentages of the three phases in the four speeds are shown in figure 8.

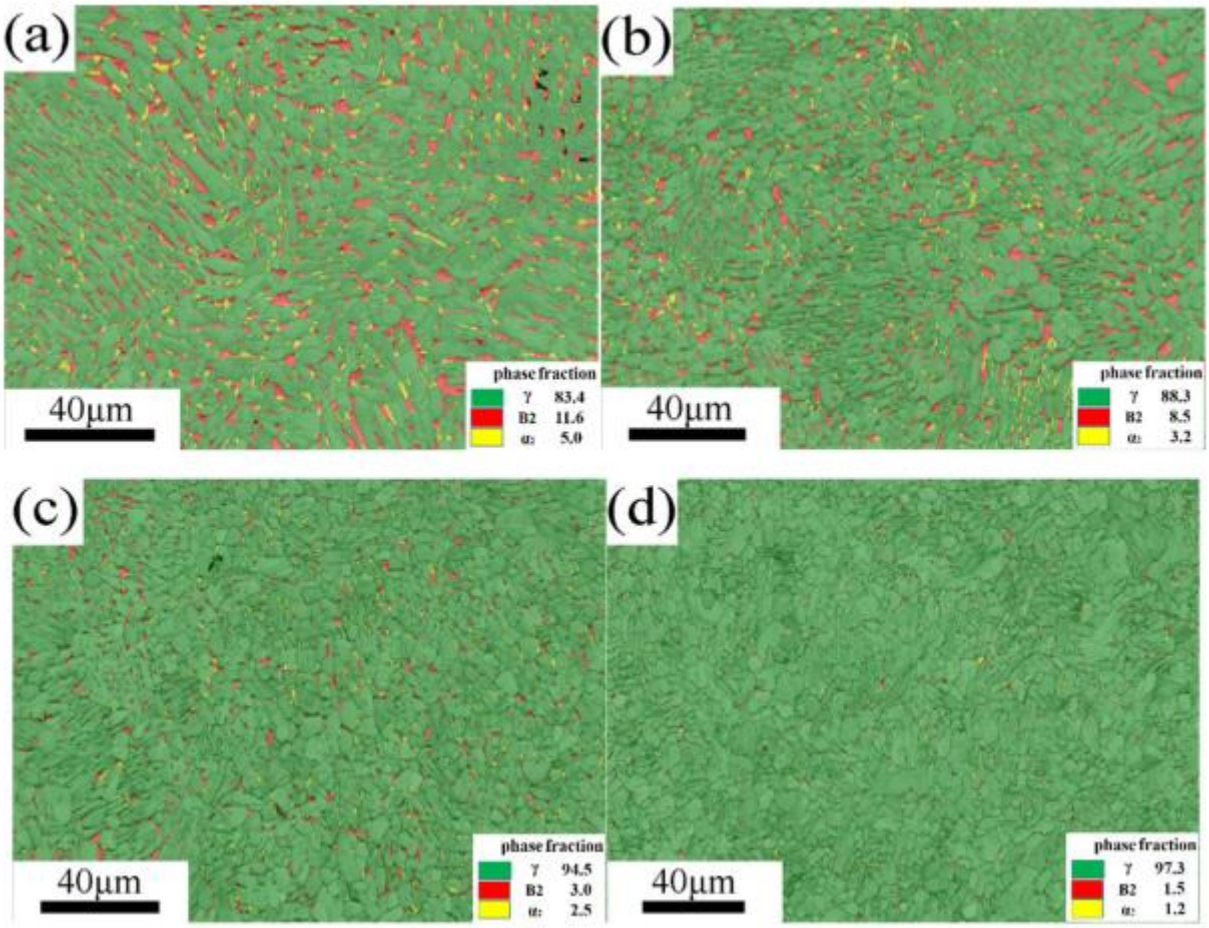

Figure 8 Image of phase maps obtained by EBSD analysis with different scanning speeds: (a) 1500 mm/s, (b) 1800 mm/s, (c) 2100 mm/s and (d) 2400 mm/s[14].

As known from the Hall-patch relationship, that describes the relationship between traction properties and grain size eq (3), a grain refinement leads to better mechanical properties.

$$\sigma_y = \sigma_0 + k_y D^{-1/2} \quad (3)$$

where σy is the yield stress, σo is a material constant for the starting movement tension of the dislocations, ky is the strain hardening rate, and D is the average diameter of the grain.

Furthermore, the ductility of TiAl alloys depends heavily on the β_2 content at room temperature. The increase in content of β_2 phase decreases ductility due to its fragile characteristic. The tensile tests confirm the theory, as can be seen from fig 9, with a grain refinement there is an improvement in the tensile properties, it is also to be observed that the samples have a better resistance than the pieces built by casting and forging (Table 2).

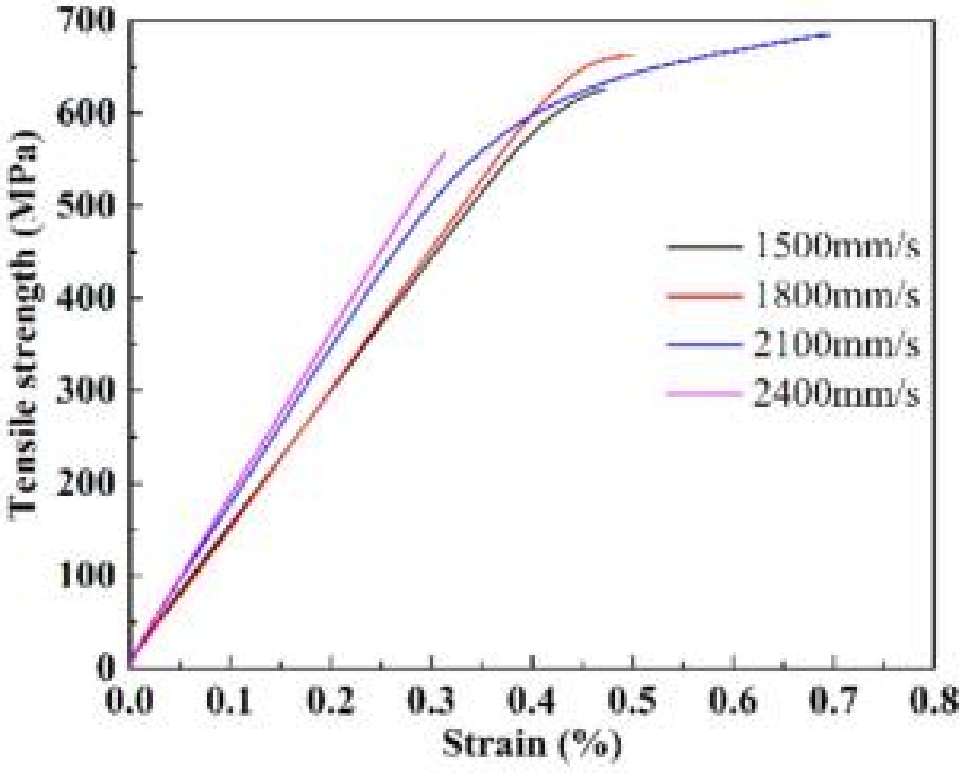

Figure 9 influence of scanning speed on tensile properties[14].

Fabricating technology	samples	UTS (MPa)	δ (%)
SEBM	S1	626 ± 8	0.47 ± 0.03
SEBM	S2	663 ± 12	0.5 ± 0.04
SEBM	S3	684 ± 7	0.70 ± 0.06
SEBM	S4	556 ± 15	0.31 ± 0.04
SEBM + HIP	–	450–500	1.0–1.2
Forged	–	557	1.3
Cast	–	570 ± 20	0.48 ± 0.05

Table 2 mechanical properties of samples processed with different scanning speed and technology[14].

All this is valid up to sample 3 and at a speed of 2100 mm/s after which with sample 4 at a speed of 2400 mm/s there is a degradation of the traction properties, even if the sample shows the greatest refinement. This is explained by the fact that there is another phenomenon at play with the increase in scan speed, the porosity.

Figure 10 shows the relationship between porosity and scanning speed. With increasing speed there is a not linear increase in porosity. For scanning speeds lower than 2100 mm / s, the presence of the porosity phenomenon is relatively low, in percentages of 0.186%, 0.243% and 0.292%, for the recorded samples S1, S2 and S3. Exceeding a speed of 2400 mm / s, the porosity rises dramatically, reaching a percentage of 0.686%, almost three times the percentage of sample S1. The phenomenon of the increase in porosity with the increase of the scanning speed is explained by the energy density. As the scanning speed increases, there is a decrease in energy density which equivalent to lower melting capacity, leaving material partially melted and irregular pores fig 10. Obviously the increase in pores leads to a

degradation of the tensile properties of sample 4, where there is a noticeable presence of pores.

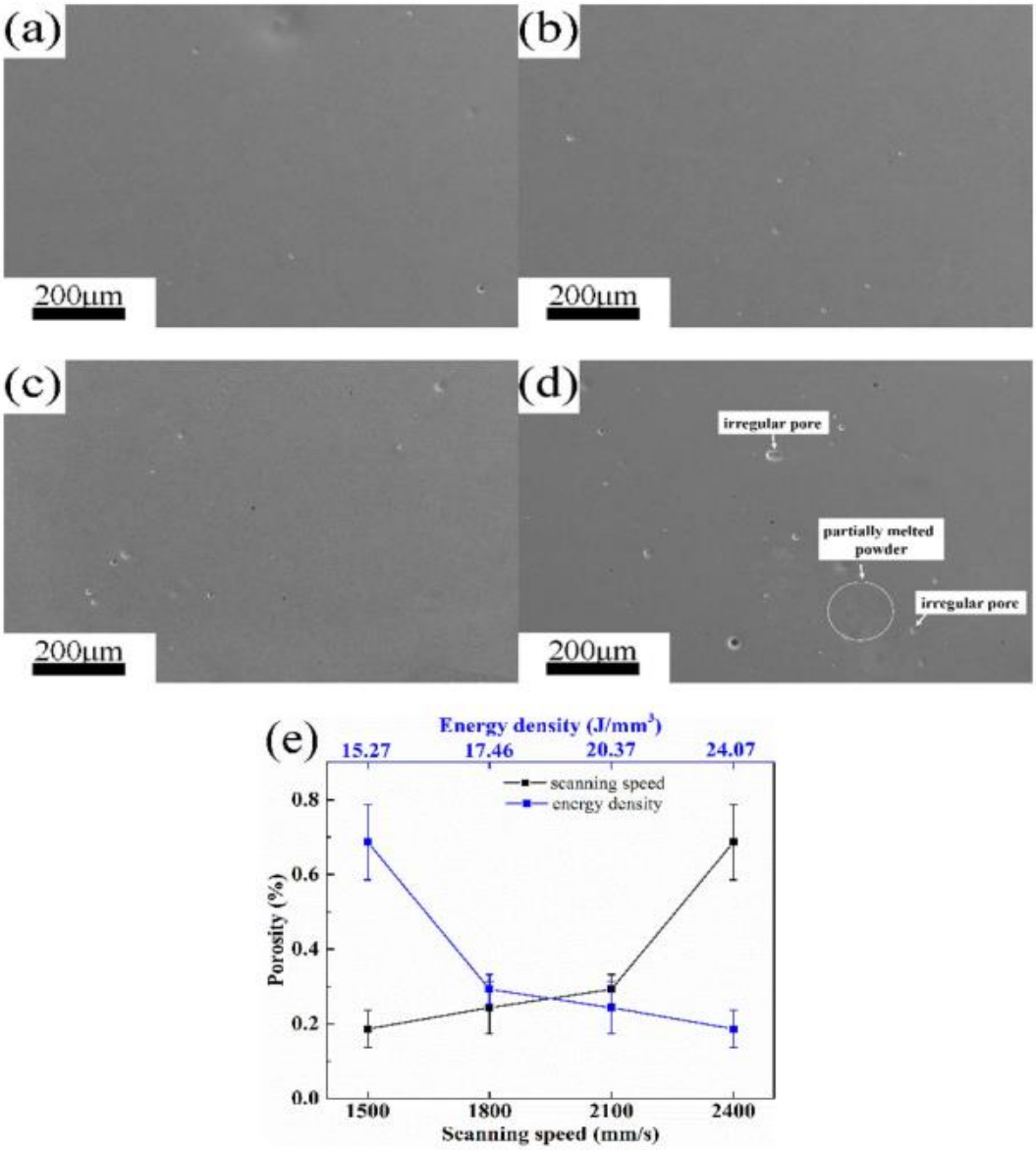

Figure 10 Sem images showing the increase of pores with the increase of the scanning speed: (a) 1500 mm/s, (b) 1800 mm/s, (c) 2100 mm/s and (d) 2400 mm/s. Figure 10e shows the relationship between scanning speed, porosity and energy density[14].

3.2 The melting strategies

it is clear that there is a strong dependence between the process parameters and the quality of the product, and in this regard it is necessary to develop a better understanding of the relationships between the process parameters and the geometry of the part, as well as the dimensions, density and distribution of the pores present inside a component, and the probability that they appear at critical points such as near the surface (fatigue strength). This information is essential for developing an effective EBM strategy. For this purpose it is interesting focus on the studies done by St. Tammas-Williams et al [10]. They did an XCT (X-ray computed tomography) analysis of the influence of fusion strategies on the population of defects in the Ti-6Al-4V components produced by Selective Electron Beam Melting. Through the XCT analysis it is possible to analyze the pores in three-dimensional space, being able to quantify the frequency, distribution, morphology and size in the titanium test samples. By varying the resolution, it was possible to study the position of the entire range of pores, as well as the actual morphology and size as the scanning strategy varied. This allowed to have very detailed and statistically relevant results, understanding the causes that give rise to the pores and their respective positions, according to the EBM construction cycle. Simple cubic samples (figure 11) were built on the base plate, in order to systematically analyze the relationship between the process parameters and the porosity levels.

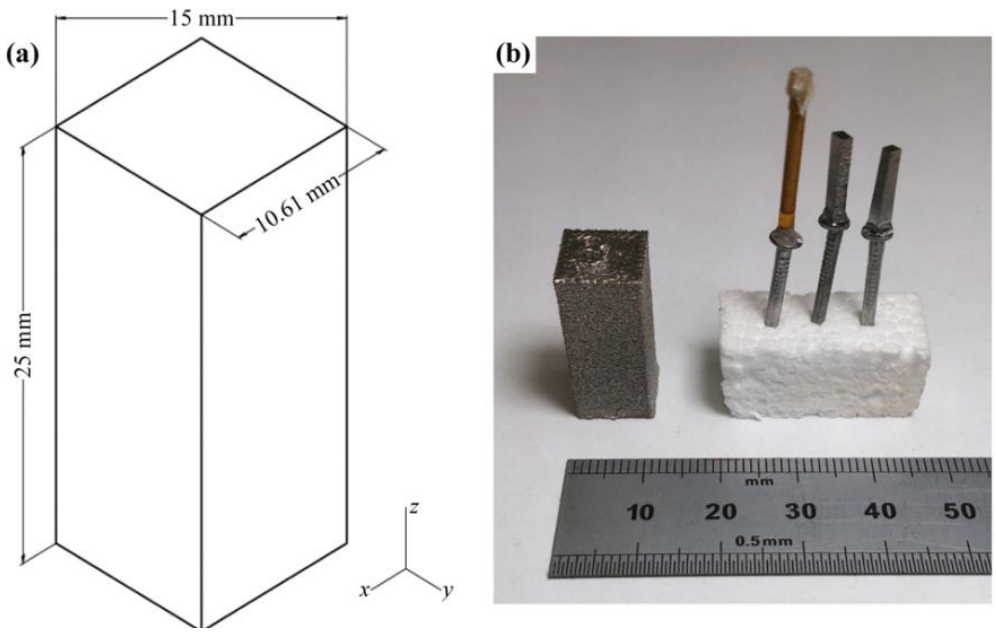

Figure 11 Geometry of the samples analyzed by XCT.

Several samples were constructed by varying the contours and the hatching strategies for each sample, in order to see their effect. In addition, other samples have been constructed so as to be able to analyze the effect of the line offset between the hatching (L0-L2), the focus offset (F0-F3) and the speed function (S0- S3), with the remaining parameters kept constant (detailed in Table 3).

Sample ID	Modification
C0	Standard settings (control)
C1	Contouring only
C2	Hatching only
C3	5 contours
C4	Contour inner to outer
C5	Hatch first
C6	Turning function disabled
C7	Single direction hatching
S0	Speed function 36 (control)
S1	Speed function 30
S2	Speed function 18
S3	Speed function 12
L0	Line offset 0.2 mm (control)
L1	Line offset 0.15 mm
L2	Line offset 0.1 mm
F0	Focus offset 19 (control)
F1	Focus offset 12
F2	Focus offset 6
F3	Focus offset 0

Table 3 Samples built with relative strategy[10].

To get a detailed overview of the process parameters used for the different samples, the table 4 shows the different values.

Process	Sample numbers	Melt length (mm)	v (begin) ($mm \cdot s^{-1}$)	I (mA)	Line offset (mm)	E_a (begin) ($J \cdot mm^{-3}$)	E_a (average) ($J \cdot mm^{-3}$)
Outer contour	All	10	280.0	5.0	0.30	51.0	51.0
Inner contour	All	9.5 & 9 (8.5 & 8 for C3 only)	700.0	12.0	0.25	58.8	58.8
Hatch	C0, C4, C5, F0, F1, F2, F3, S0, L0	9	324.3	5.7	0.20	75.5	48.4
	C2	10.6	371.7	6.1	0.20	70.8	48.4
	C3	8	294.7	5.3	0.20	77.2	47.8
	C6, C7	9	324.3	5.7	0.20	75.5	75.5
	S1	9	254.6	5.7	0.20	96.1	59.4
	S2	9	185.3	5.7	0.20	132.1	78.9
	S3	9	115.9	5.7	0.20	211.2	122.9
	L1	9	327.0	5.7	0.15	100.5	64.6
	L2	9	327.0	5.7	0.10	150.8	96.9

Table 4 process parameters for the different samples [10].

As can be seen from table 4 there are different values of current and speed between samples C0 and samples C2 and C3. This is because the contour passages have been added or removed in the various samples, leading to longer or shorter hatches. The control software assigns higher currents to longer hatches and lower currents to shorter hatches, in order to give less power (voltage is kept constant) to smaller pools. In addition, to keep the depth of the different pools constant, the I / v ratio is kept constant, therefore the increase or decrease in current leads to a corresponding increase or decrease in speed [10]. Instead for the S1-S3 samples, the speed function was deliberately reduced, leading to significant changes in energy density due to the speed variation. In addition there is another important function set in the EBM called turning function. This function has been designed to avoid overheating in the area where the hatch trace is reversed, increasing the beam speed and avoiding the accumulation of heat in the area recently melted by the previous passage. With rotation, the increase in speed is controlled by an exponential function with parameters the distance from the previously melted area and the initial speed, while the power of the beam is kept constant [10]. With increasing speed without increasing the beam power there is a decrease in energy density. The effect of the rotation function can be observed in Fig. 12, comparing the samples C0 and C6, where the rotation function has been enabled and disabled respectively, keeping the remaining settings constant. The diagrams of figure 14 show that the rotation function maintains a speed higher than the initial over the entire width of the section, and even if it decreases with increasing distance, it never goes back to its initial speed, the phenomenon is equivalent for energy density (identical to line C6). Therefore, the average of effective energy density is less than the values calculated, based on the initial speed in the table. The estimated effective average hatch energy was therefore also included in table 4.

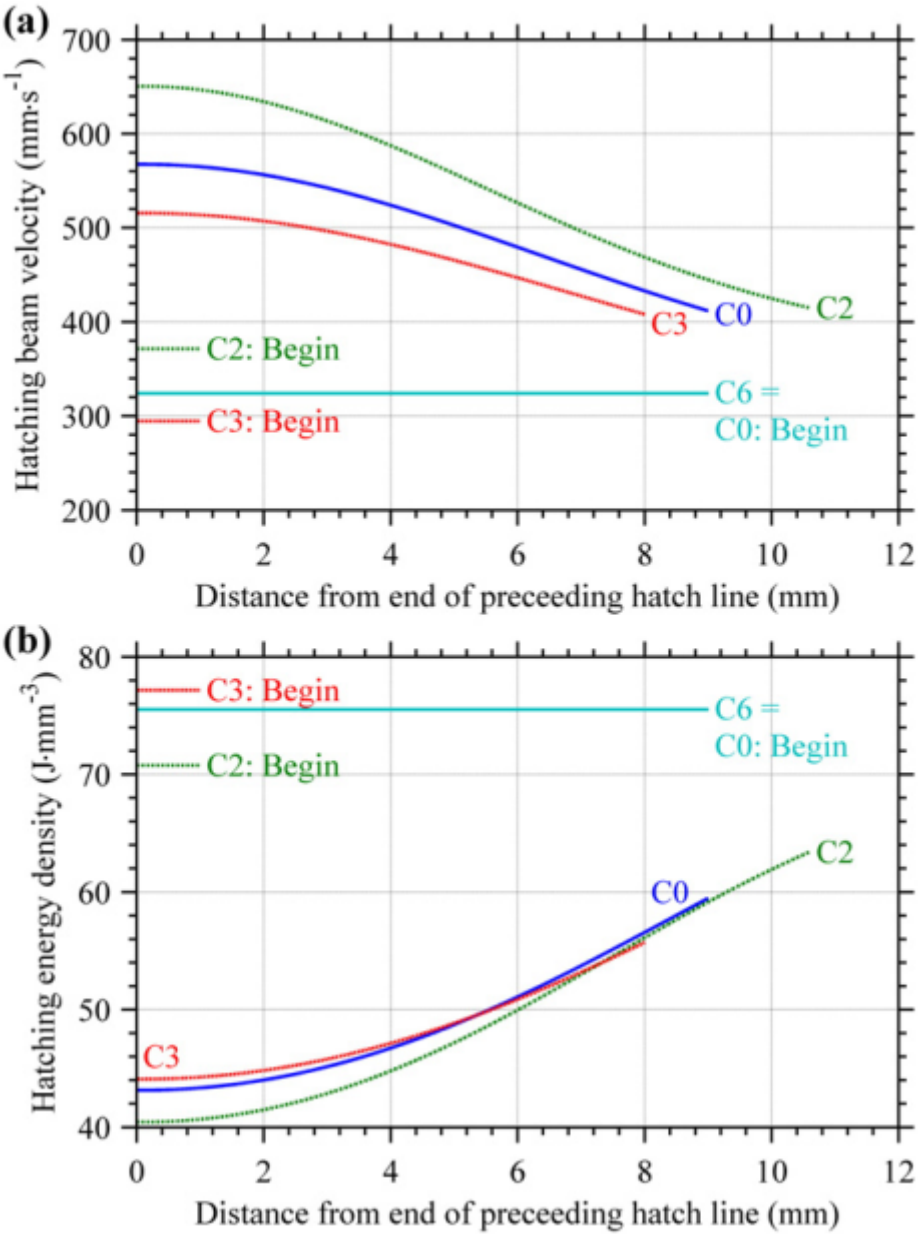

Figure 12 the effect of the turning function on the beam speed (a) and on the energy density (b).

Figure 13 shows the pore frequency size distributions obtained from the XCT by scanning the entire C0 sample (with a voxel size of 10 µm) and on machined sections of 1.6 mm (with a voxel size of 2 µm), from the centre and edge of the same sample. In addition the data obtained from conventional 2D metallographic optical microscopy measurements of pore sizes are compared. To allow for a better

comparison, the optical results were converted into an equivalent volume distribution using the Schwartz - Saltykov (S - S) analysis [10]. Overall, the comparison between the three distributions shows that most pores have a diameter of <100 µm and few (~ 0.02 for mm^3) exist over 150 µm in size.

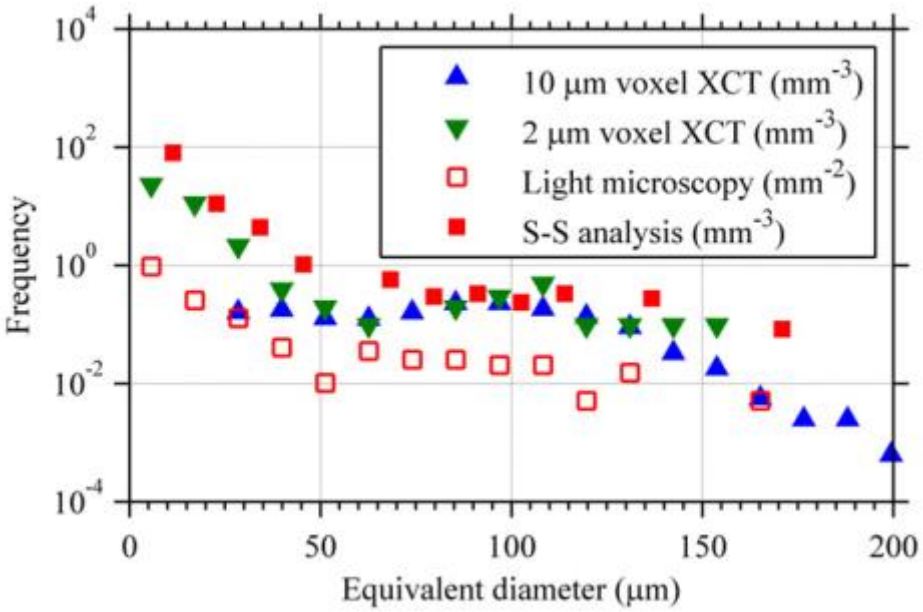

Figure 13 proportions obtained from the standard sample C0 from XCT high resolution data taken on board and in the center of the sample and lower resolution data from the whole sample, plotted as ratio frequency distributions[10].

Figure 14 shows some examples of pores detected with SEM analysis in the x-y plane (construction plane). In the comparison, figure 15 shows the different pore morphologies represented by XCT.

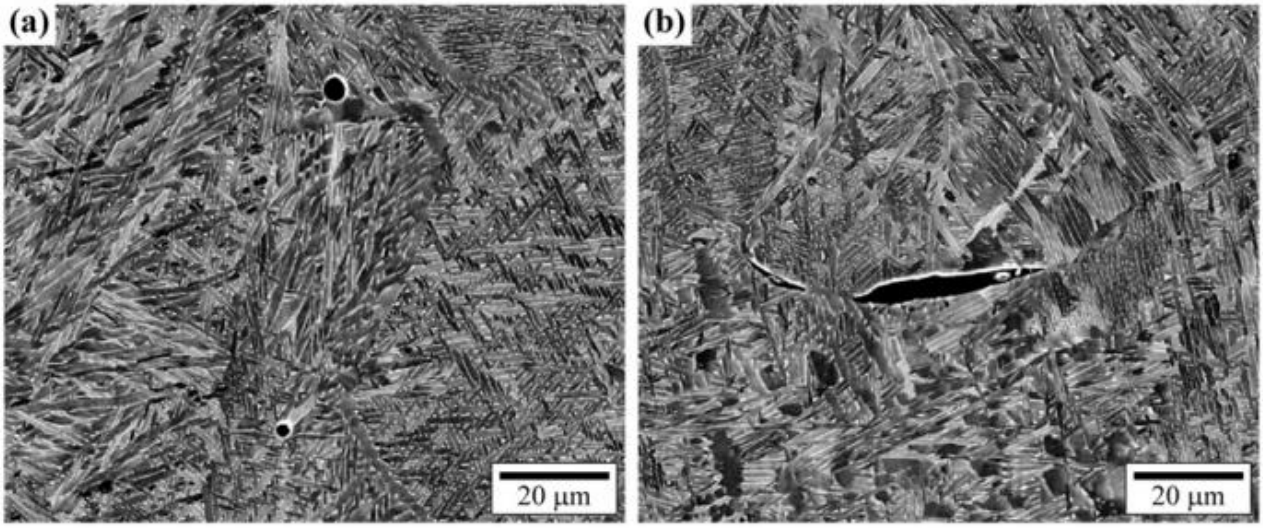

Figure 14 Examples of pores detected with SEM analysis in the x-y plane (construction plane).

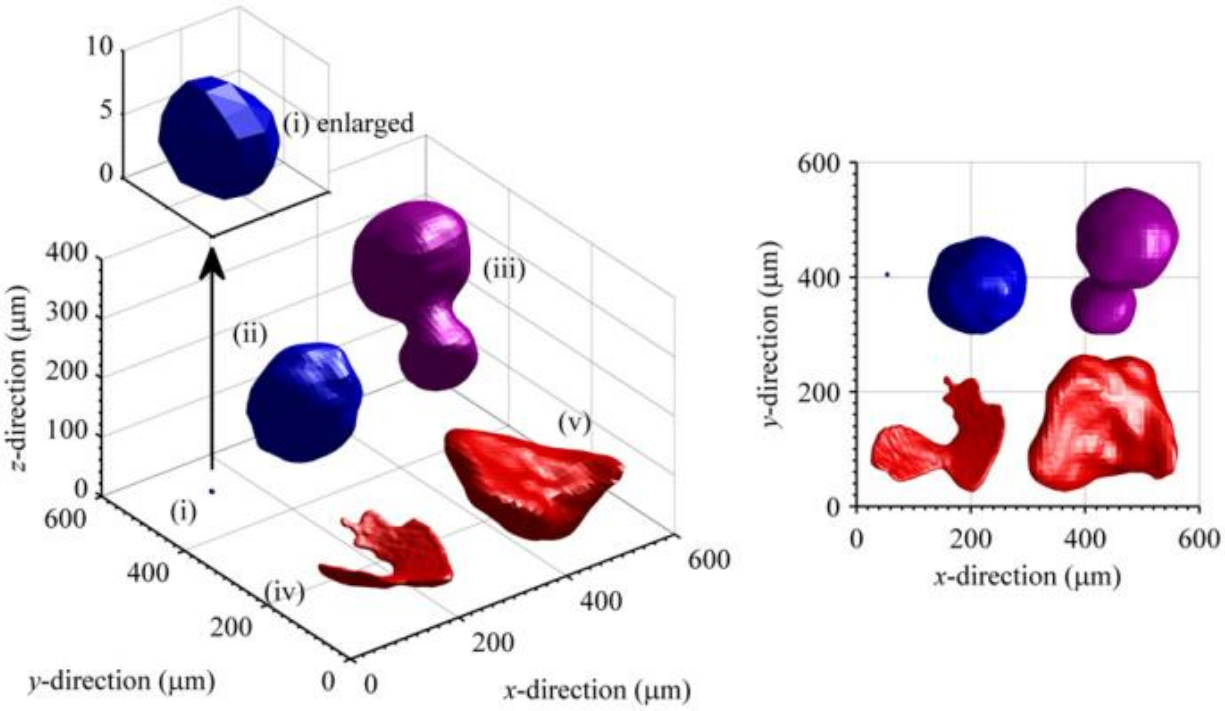

Figure 15 Examples of pore types detected by XCT in the standard sample, C0, on the same scale: spherical pores, small (i) and large (ii) (blue); (iii) two near spherical pores joined together (turquoise); irregular pores, small (iv) and large (v) irregular (red). The build direction is z while x and y denote the hatching directions.

Figure 14a shows the common circular pore observed with a size between 5 and 160 µm, these pores correspond to the pore 'i' and 'ii' in the recruited XCT analysis shown in figure 15. Figure 14b instead shows the rare lack of fusion defect detected by SEM equivalent to the type IV defect shown in figure 15. Furthermore, the XCT analysis of the entire CO sample revealed a rare irregular type V pore near the edge with a size of about 190 µm. However, this type of defect was not detected by the SEM analysis due to its low frequency. It was also observed (figure 16) that there was a greater frequency of irregular pores near the edge. On the contrary, within the dotted region the center of the sample contained few irregular pores, but a greater number of spherical pores. However, most of the pores identified in both specimens were small (<75 µm) and spherical.

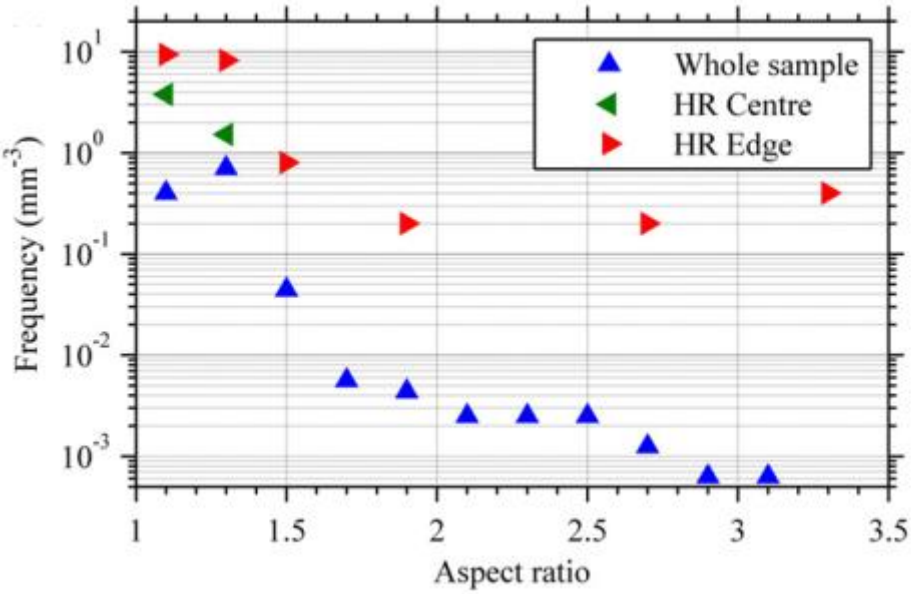

Figure 16 frequency distributions of the ratio between the main axes of the pores on the edge (HR edge) and in the center (HR center).

Given the different nature and frequency of the pores on the edge and the center will further study is carried out by varying the melting strategy in the different samples, in order to understand the causes. Figure 17 shows the pore frequency as a function of the distance from the surface, highlighting the extent of this phenomenon for the standard sample C0.

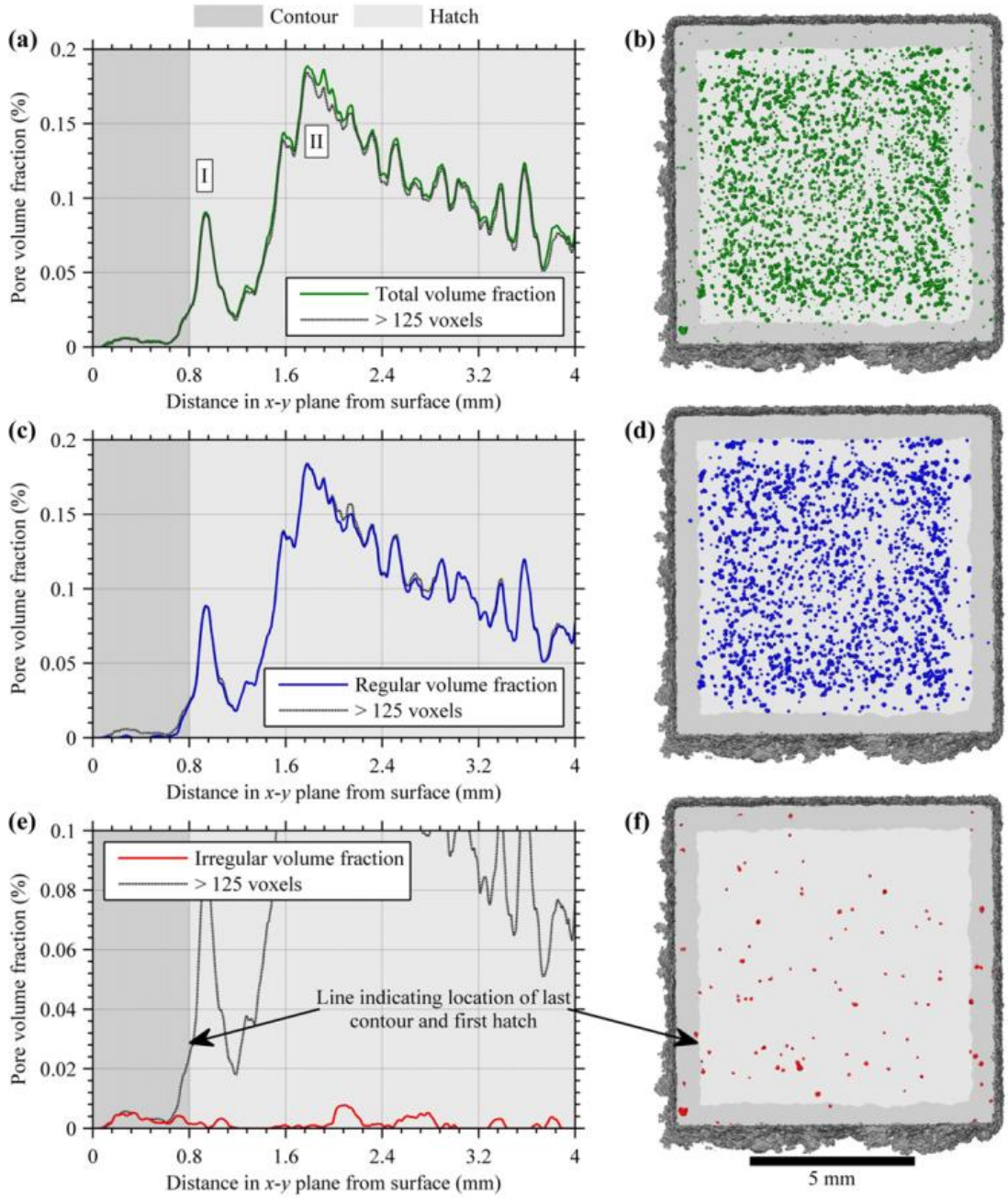

Figure 17 Pore frequency as a function of distance from the surface for sample C0 (a)the variation in the total pore volume fraction; (c) distribution of regular pores only (e) irregular pores, (b,d,f) qualitative visualization in the x-y plane [10] .

As can be seen, there is a higher frequency in the center of the sample while in the contouring area there is a lower frequency. Furthermore, moving away from the edge, two peaks can be seen. The first called "I" at a distance of 0.8 mm from the surface, coincides in the area between the inner contour and the outermost hatching, and the second "II" at about 2 mm from the surface which coincides in the hatching area. To understand the nature of the phenomenon and the influence of the process strategy, the same analysis was performed with all the samples with different strategies (figure 18-19). As can be seen from the different results of the samples analysis, the fusion strategy has a significant influence on the distribution and type of pores. An example is the sample C1 (contour only) which showed a much lower pore frequency and absence of peaks. While C2 (hatching only) has a much larger pore frequency, with peak II shifted by a distance of 0.8 mm equal to the additional hatch length required when contouring has been disabled. It is evident that peak II depends exclusively on hatching.

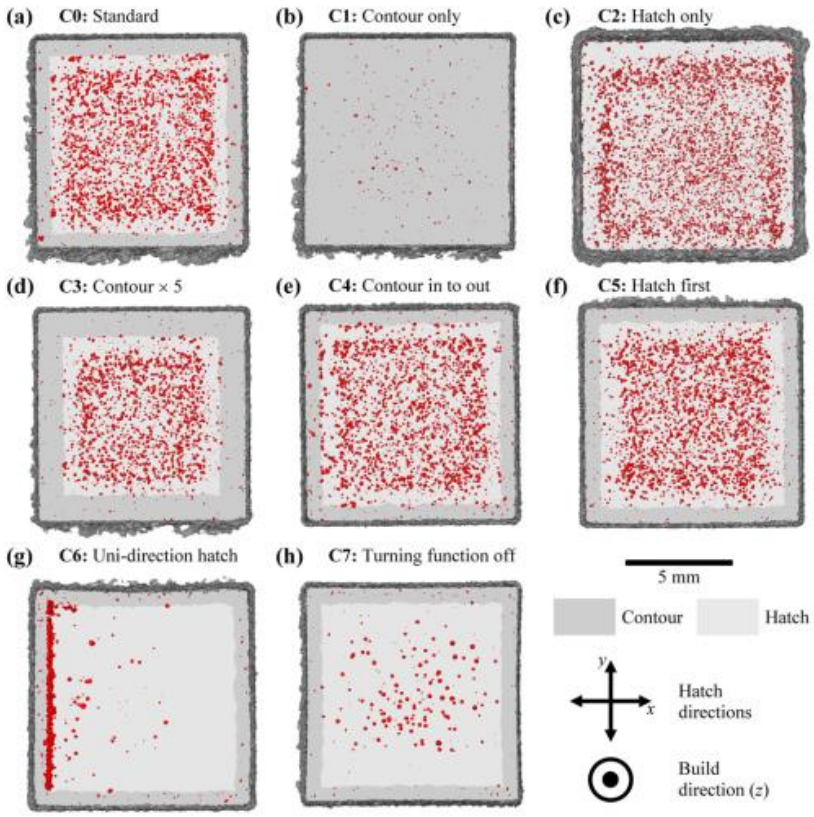

Figure 18 frequency and distribution of pores as the melt strategy changes[10].

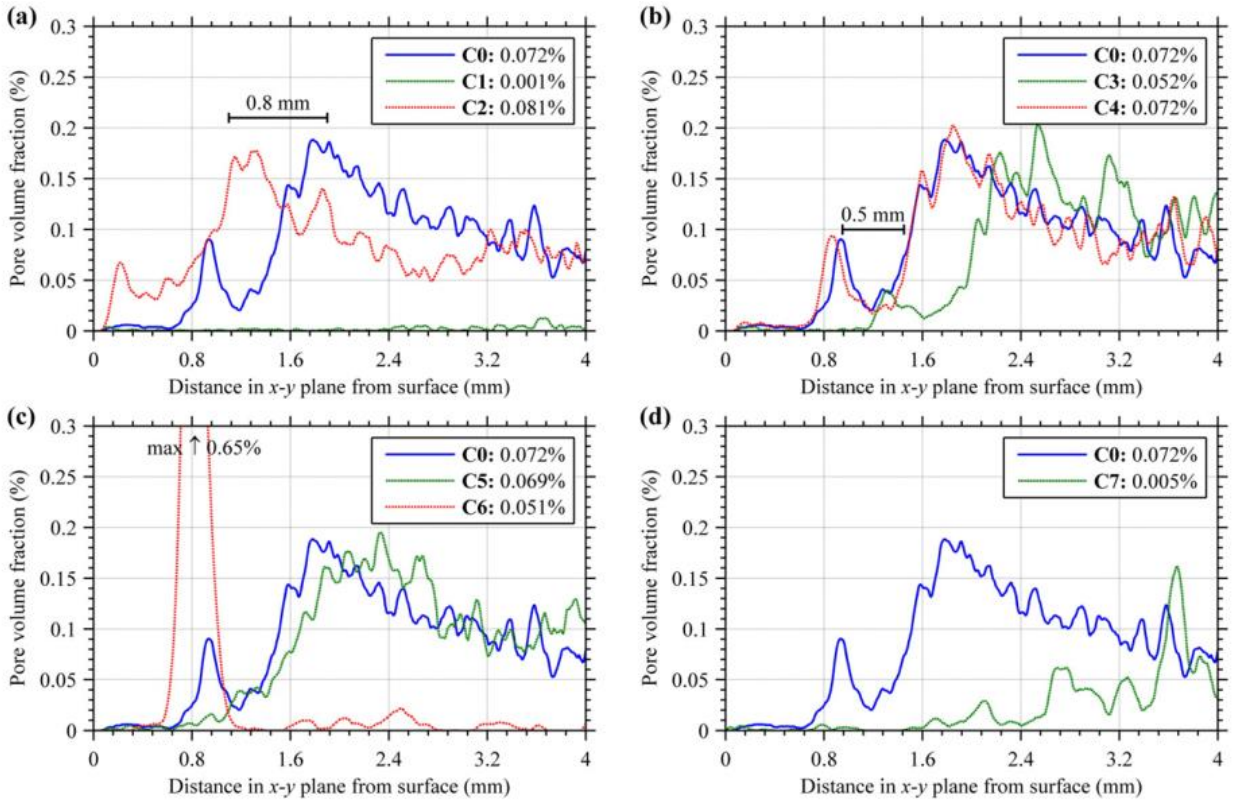

Figure 19 Effect of the process change, compared to the recommended standard settings (sample C0), distribution of the pore volume fraction with the distance from the construction edge[10].

With regard to the peak I from the sample C3, where the contour has been increased from 3 to 5, it can be noted that the peak I is moved exactly the extra distance occupied by the 2 additional contours (2 x 0.25 mm). Furthermore, when the hatching was performed before the contour (sample C5) the peak I was not noticed. Moreover, If the hatching is performed in one direction only, by deactivating the "snake" function, the peak I becomes very pronounced, in contrast with the peak II which is absent. The disappearance of the second peak in sample C5 is probably caused by the hatching in one direction, automatically deactivating the turning function. To confirm this hypothesis, sample C7 was analyzed with normal hatching but with the turning function deactivated. Again, the pore density in the hatching area was significantly lower. From the experimental data, it is evident that these two pore concentration positions are clearly related to the edge of the hatch lines. The I peak is caused by the

fact that the pores, pushed from the solidification front, are discharged at the end of the hatch, and this also occurs if the turing function is activated in the standard hatch strategy. While peak II inside the hatch area, is probably caused by the turnig function, which by increasing the beam speed, causes a decrease in both the time available and the energy density, not allowing the gas bubbles to escape. In addition, due to the increase in speed of the rotation function, there will be much narrower and shallower fusion pools, not allowing an adequate overlap of the fusion tracks. [10]. These pores, with their mainly spherical morphology, derive from trapped gas bubbles, which failed to escape during solidification. As the process takes place in a vacuum, it is believed that these gas bubbles do not derive from the type of process, but are intrinsic in the powder used, due to the use of trapped argon during the manufacture of this powder by plasma atomization, In confirmation of this, virgin powder was also analyzed, detecting a significant level of pores inside larger dust particles (figure 20).

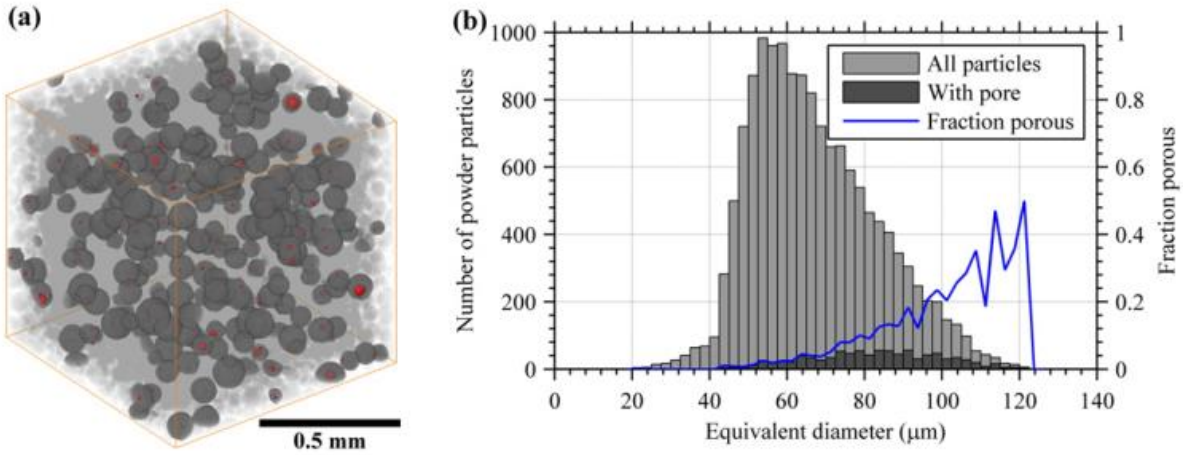

Figure 20 a) XCT virgin dust analysis shows the presence of gas pores. b) Distribution of all particles and those that contain pores, the fraction of pores for each size of powder is also indicated.

As for the contour, it is true that it has the lowest pore frequency, but most are irregular pores which are the most harmful for the fatigue life of the piece. A possible

cause of this irregular pores, with a size ranging from 18 µm up to 190 µm, could be the MultiBeam, which by simultaneously keeping 10 fusion pulls active, could lead to instability, not allowing the material to melt completely. In addition, the contour with respect to the hatching, uses a more focused beam, generating much deeper pool but but tight, failing to ensure a sufficient overlap between the passages. In any case, the relationship between the focus offset and the volume fraction of the pores is far from simple. Figure 19 relates the focus offset to the porosity fraction. When the focus offset is reduced, from its standard value (F0: Focus offset = 19 mA) there is an initial reduction of the pore volume fraction by an order of magnitude, continuing there is an increase again of the pores when the focus beam was at the maximum (F4: focus offset = 0 mA).

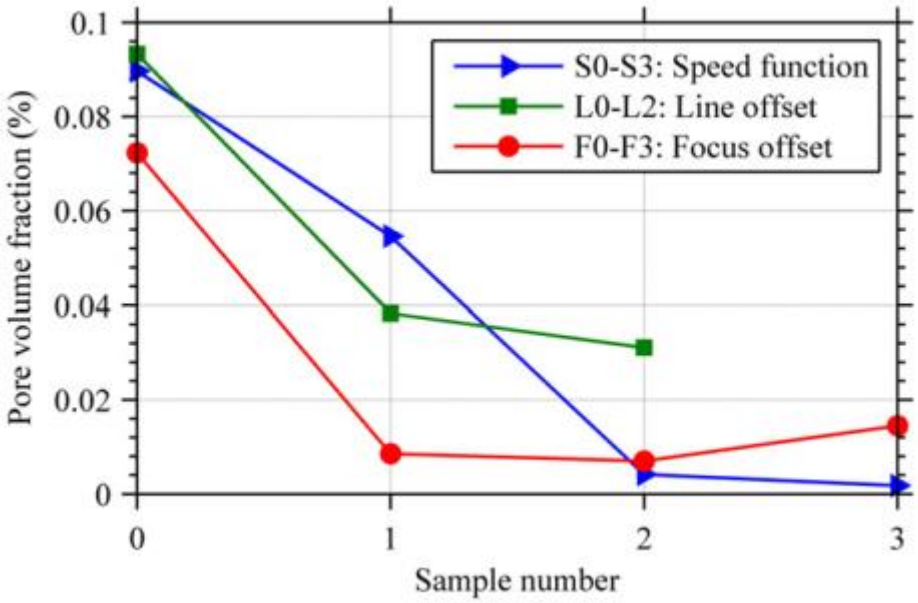

Figure 21 Influence of focus offset on porosity [10].

Figure 21, in addition to the focus offset and the previously discussed scan speed, shows the dependence of porosity with the line offset. It is evident that the reduction of the line offset leads to a reduction of porosity.

3.3 Energy density

To further understand the phenomenon and simultaneously analyze the effect of different process parameters it is useful to study the effect of energy density on porosity, being an excellent benchmark parameter. Figure 22 shows the inverse relationship between porosity and mean energy density. Which as previously discussed, it was calculated by integrating the beam speed along the entire length of the hatch, also including the contribution of the turning function, and considering the corresponding effects of the contour and hatching in a proportional way [10]. The analysis shows that a higher energy density leads to a deeper and larger fusion pool, this guarantees a better overlap and recast between the different passes, facilitating the escape of the gas bubbles [10]. In addition, it is evident from the results, that by increasing the energy density above the standard settings recommended by Arcam, the volume fraction of both the gas pores and the defects caused by the lack of fusion, is significantly reduced.

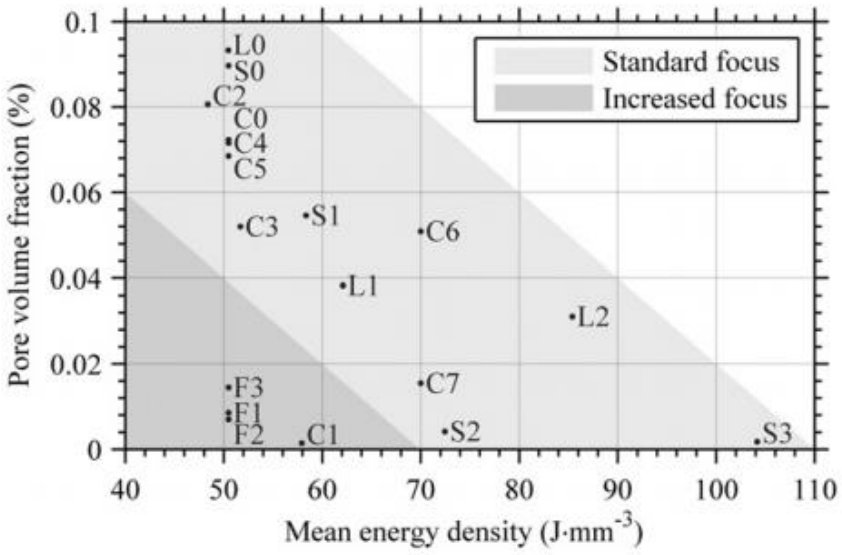

Figure 22 Relationship between average energy density and porosity in the different samples.

3.3.1 The problem of aluminum evaporation

The increase in energy density has some drawbacks. In addition to increasing operating costs, a high energy input in the EBM process can lead to a high evaporation of the elements, in particular the loss of aluminum elements, with a relative mass decrease of the aluminum component in the samples of 2% -7% compared to the original powder [16]. So even if there is a decrease of pores, the decrease of Al in turn, influences the microstructure and mechanical properties of the alloy. In this regard, it is useful to analyze the studies done by Jun Zhou et al, on evaporation in Ti47Al2Cr2Nb samples [16]. Figure 24 shows the relationship between the increase in energy density and the effect of the loss of the aluminum ratio on square samples at a vacuum pressure of 1 Pa. The results confirm the hypothesis that an increase in energy input leads to a decrease in aluminum. When the energy density reaches 22.8%((with a speed of 250 mm/s and a current of 12 mA), the aluminum loss is 15.8%. Furthermore, decreasing the pressure, the effect is considerably widened (figure 25).

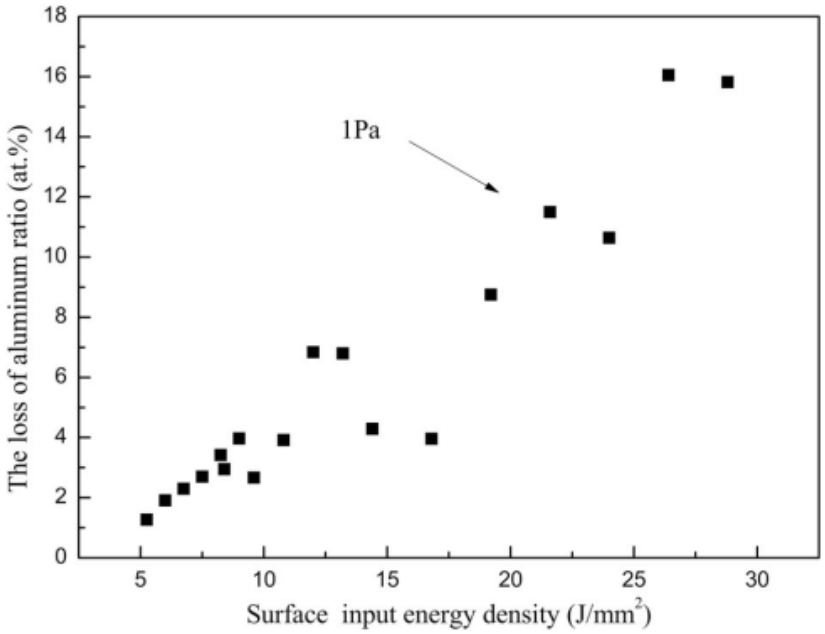

Figure 23 Effect of surface input energy density on the evaporation of aluminum at the pressure of 1Pa.

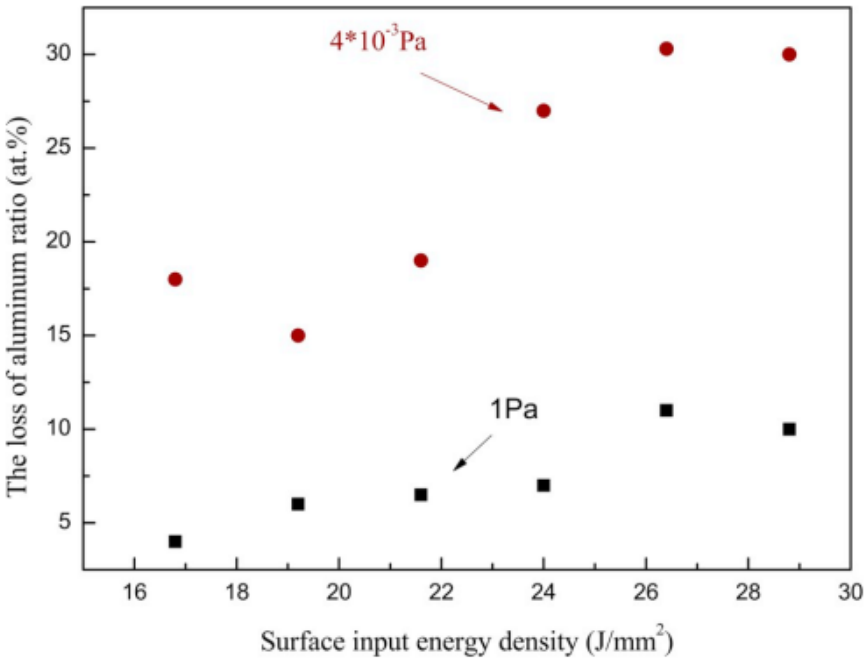

Figure 24 effect of different pressure on the evaporation of aluminum.

The relationships between saturated vapor pressure of titanium and aluminum elements and the temperature can be calculated using the following equation (4) :

$$\log P_{Ti} = log_{10}133 + (-23200T^{-1} - 0.66\ log_{10}T + 11.74) \quad (4)$$
$$\log P_{Al} = log_{10}133 + (-16380T^{-1} - 1.01\ log_{10}T + 12.92)$$

To which it is necessary to take into account the atomic ratio of each element to calculate the effective pressure eq (5):

$$P_i^0 = x_i y_i P_i \quad (5)$$

With x_i, the atomic ratio of the element binds in the alloy, y_i the activity coefficient of the element set equal to 1 and P_i the corresponding pressure that the element would have if it were alone. To calculate the evaporation rate of each element the Langmuir equation (6) can be used.

$$j_i = \frac{\delta P_i^0 M_i}{\sqrt{2 M_i \pi R T}} \quad (6)$$

With j_i the evaporation rate of the i th element (Kg / m2 · sec), M_i molar mass of the i th component (Kg / mol), *R* the universal gas constant (R = 8.314J / K · molar), T the temperature expressed in degrees K, and δ is an evaporation coefficient, which depends on the degree of vacuum with values of 0.2 and 1 at vacuum pressures of 1 and 4 × 10−3 Pa, respectively. As can be seen by interpolating the equation (see figure 2) the evaporation rate of titanium is almost zero, while the evaporation rate of aluminum is significant.

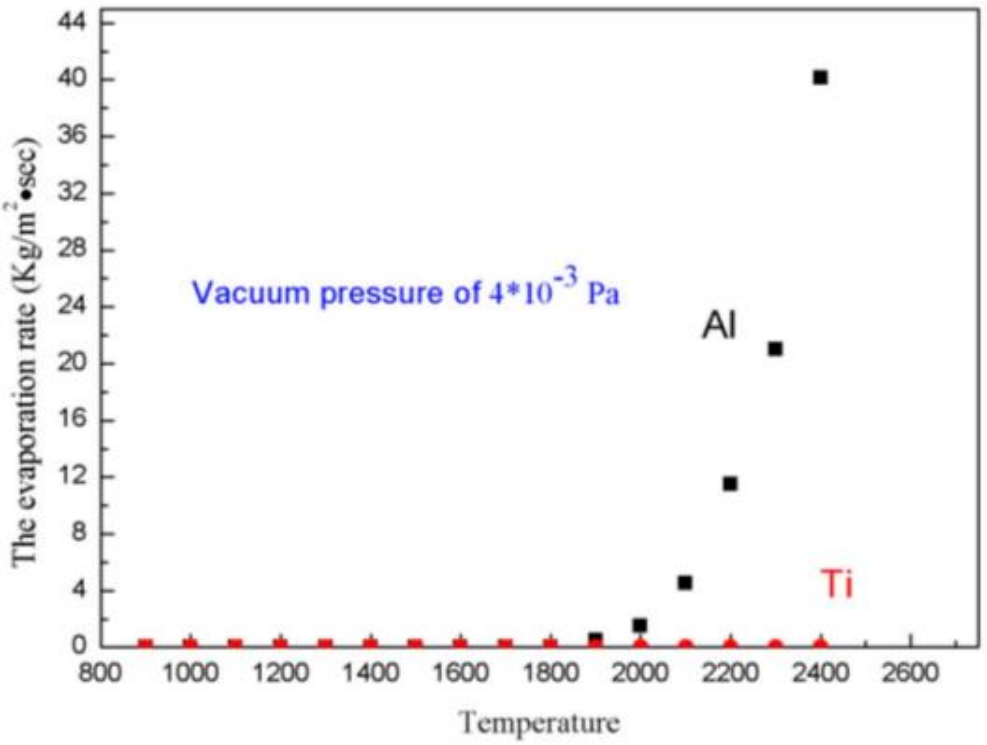

Figure 25 evaporation rate of Ti and Al at pressures of $4 \cdot 10^{-3}$.

4 DIMENSIONAL AND ROUGHNESS CHARACTERISTICS IN THE EBM PROCESS

In this chapter all factors that influence dimensional accuracy and roughness in the parts produced by EBM will be analyzed. Specifically, after discussing surface roughness, greater emphasis will be given on dimensional and geometric accuracy. There is not much in the literature on this study, especially for titanium aluminide, and the purpose of this thesis is to provide a systematic view of how melting strategies in the EBM, can affect these characteristics.

4.1 The roughness

The process parameters not only influence the microstructure, but also the roughness of the product. Roughness is a very important factor, especially for the fatigue life of

the piece. Numerous studies have confirmed that the nucleation of the crack occurs near the surface due to roughness. In the literature, there are no large studies on the roughness of the titanium aluminide, but the study of the Ti - 6Al - 4V alloy produced by EBM can be a good example. Several analyzes showed a relevant roughness in different EBM samples. For these products the Ra parameter, surface roughness index, varies from 1 to 20 µm, based on the settings of the thickness and the remaining process parameters. The presence of a high roughness is not always a negative problem, but depends on the application field. For example, in the previous paragraphs it was mentioned how EBM is applied in the biomedical field. Through this technique, it is possible to customize the single orthopedic or dental prothesis for the patient by designing and building it through CAD and EBM process. Furthermore, titanium alloys have a large success in this field thanks to the mechanical and physical properties such as biocompatibility, specific resistance and corrosion resistance. In this application for example, have certain levels of roughness favors interaction with human tissue. The speed and quality in the formation of new tissues depends on the surface properties such as chemical, energy, topography and surface roughness of the material. Studies in this field have shown that the use of rough titanium surfaces has led to higher levels of cell attachment and greater collagen production [17]. However, these cells are able to discriminate even small differences in surface roughness, and for this reason that the process and the final roughness of the parts must be well controlled. Nevertheless in other applications, such as in the aerospace sector where titanium alloys finds application in the last turbine stages, it is important to maintain low roughness values, with Ra index about 1.5 microns. In addition, various studies in this field have shown that the simple Ra index is not enough to optimize the vanes. There is a need to specify other aspects of roughness to handle phenomena such as skin friction resistance or the heat transfer rate on the vanes, through the Ks parameter “the equivalent sand grain roughness height”. This parameter is defined as the height of roughness that would have produced the same skin friction for a sand

grain surface, and it is sensitive to both the spacing of the roughness elements and the shape of the element [18]. From the non-exhaustive examples discussed, it is clear that the systematic analysis of all the phenomena that influence roughness in the EBM process is essential. By choosing the right combination of parameters, it possible to obtain the desired roughness in a controlled way. Roughness has a set of parameters opposite to the porosity problem. The Ra value decreases with increasing focus offset and beam speed, on the contrary with an increase in the thickness of the sample or the beam current, the roughness parameter increased. In this regard, it is useful to analyze the experiments conducted by A. Safdar et al [19]. In their studies, they have implemented a multiple regression model to capture the influence of process parameters on roughness, with an equation of the type eq (7).

$$Y= \beta_0+\beta_1 X_1+\beta_1 X_2+\beta_1 X_3+\ldots . \beta_n X_n+ e \quad (7)$$

In this case, the use of the first order model to approximate a function is valid only if the same function does not show a trend far from linear and only if it is used for a not too large interval. Once the equation has been obtained, it is possible to select the best combination of the different parameters including the thickness, and obtain the desired roughness. There are several parameters to analyze the roughness, in this study the parameter Ra was used, obtained by making the arithmetic mean of the absolute values of the deviation of each point from the average line. In this study four sets of rectangular test plates comprising contours and squares were examined. Each set consists of three blocks of approximately 55 × 50 mm in their respective X and Y directions. The plates were produced with Ti - 6Al - 4V powder with a size of 50-100 µm. Figure 26 schematically illustrates the samples.

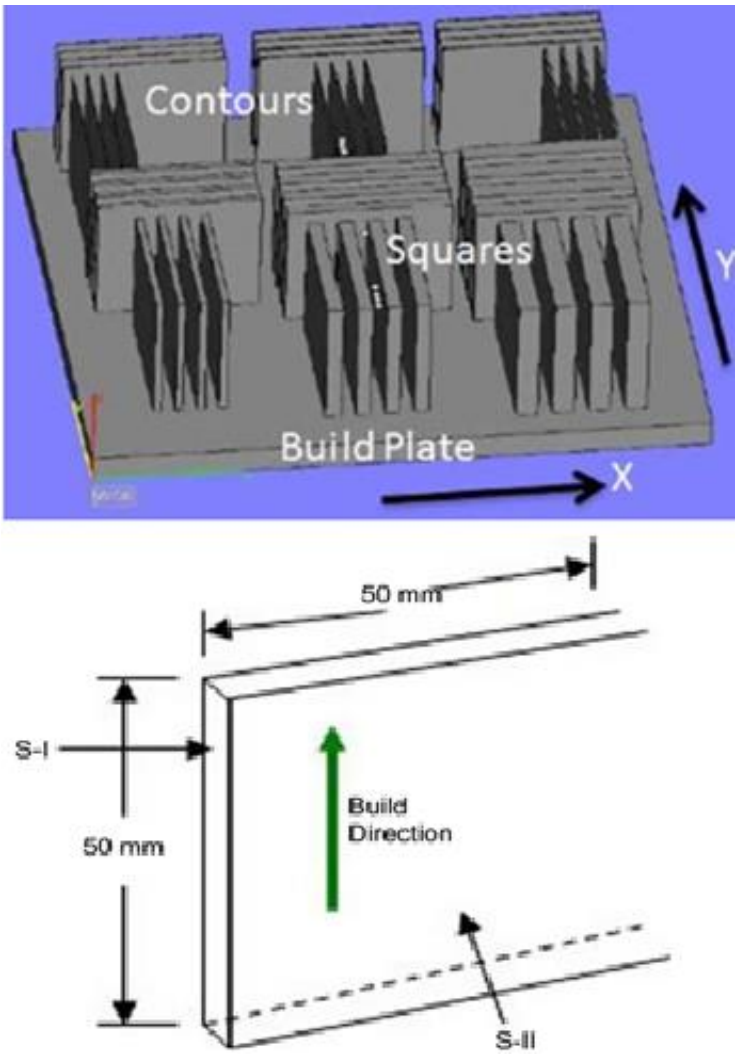

Figure 26 schematic representation of the series of samples, and of the single plate.

Each set has been constructed with different parameters and each block of the set has a different thickness (w). In addition, the samples were built to have a set of similar parameters except one, in order to study the influence of the individual process parameters. Table 5 lists the set of parameters for different samples.

Theme/part	Scan speed (mm/s)	Current (mA)	Offset focus (mA)
Contour 1	250	4	10
Contour 2	250	6	10
Contour 3	250	4	25
Contour 4	250	6	25
Square 1	180	8	15
Contour			
Square	575	9	15
Square 2	180	8	15
Contour			
Square	650	9	15
Square 3	180	8	30
Contour			
Square	575	9	30
Square 4	180	8	30
Contour			
Square	650	9	30

Table 5 process parameter for each set [19]**.**

To study the influence of various processing parameters, they are chosen such samples with similar builds, except for the parameter of interest to be studied. The selected samples are shown in table 5.

S. no.	Sample no.	Width (mm)	Scan speed (mm/s)	Focus offset (mA)	Current (mA)	Experiment
1	C1X2	2.09	250	10	4	Current
2	C2X1	2.10	250	10	6	
3	C1X1	1.29	250	10	4	Thickness
4	C1X3	1.59	250	10	4	
5	S1X1	3.50	180[a]/575[b]	15	8[c]/9[d]	Thickness
6	S1X3	7.42	180/575	15	8/9	
7	S3X3	7.42	180/575	30	8/9	Offset focus
8	S1X3	7.46	180/575	15	8/9	
9	S2X3	7.37	180/650	15	8/9	Scan speed in squares
10	S1X3	7.42	180/575	15	8/9	

Notes: [a]Scan speed for the contour part; [b]scan speed for the square part; [c]beam current for contour part melting; [d]beam current for the square part melting

Tabele 5 Selection of samples for comparative studies[19]

To guarante the same conditions, all the samples were built in the same job. With a construction temperature of 700 ° C, a vacuum level of 10^{-4} Pa and with the use of helium as an inert gas

For this study, they have been of great interest, the plane parallel to the direction of building Z, indicated with S1 (the short side) and S2 (the off side), illustrated in Figure 28. From the SEM analysis on the surfaces, powders attached to the surface due to partial melting or sintering have been found. These powder particles contribute significantly to the production of rough surfaces (figure 29).

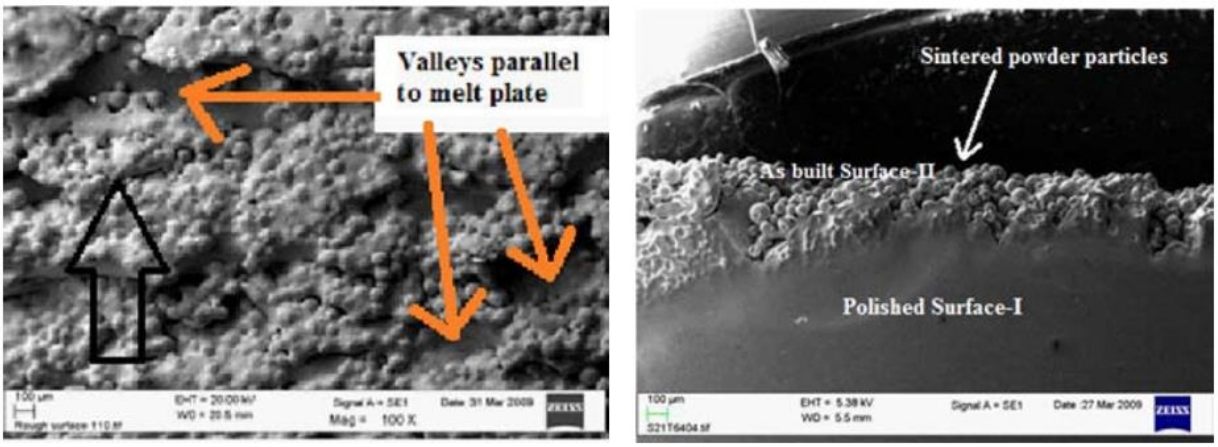

Figure 27 SEM scan of surfaces parallel to the direction of construction, a surface S II, b surface S I [19]**.**

The SII surface consists of valleys, parallel to the melting plate with varying depths and widths. Furthermore, it should be noted that the distance between the valleys is greater than the thickness of the layer. As for the cross-sections of the S-I, it is possible

to observe a surface with an inharmonic structure consisting of a mountain valley, caused by the overflow of the joined pool (figure 30).

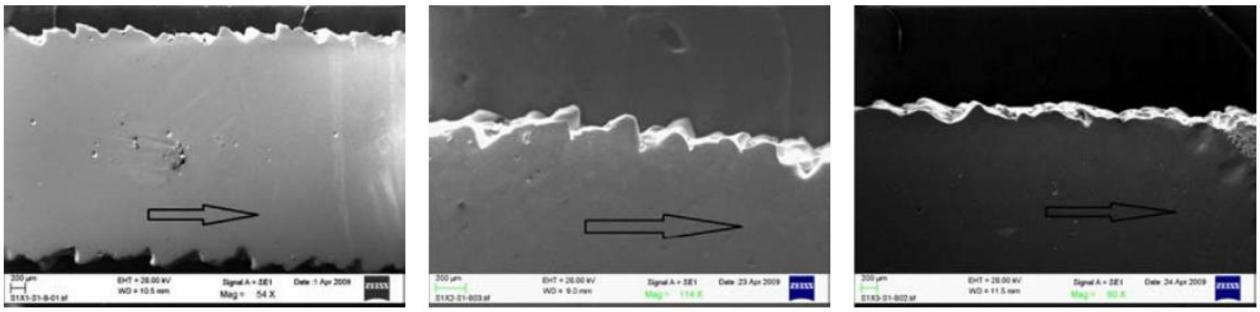

Figure 28 Cross section of the S-I, for samples with a thickness of (a) 3.5 mm; (b) 5.5mm; (c) 7.5 mm [19]**.**

The result of the Ra parameter obtained in the different samples is summarized in the table 6,

Parameter	Sample name	Parameter value	Avg. R_q (μm)	Avg. R_a (μm)
Thickness	S1X2	5.42 mm	10.57	4.29
	S1X3	7.42 mm	19.04	9.98
Thickness	C1X1	1.29 mm	18.85	7.92
	CIX3	1.59 mm	29.72	17.25
Current	C1X2	4 mA	12.07	4.45
	C2X1	6 mA	19.83	7.72
Scan speed	S1X3	575 mm/s	19.04	9.98
	S2X3	650 mm/s	12.98	5.77
Offset focus	C1X3	10 mA	29.72	17.25
	C3X2	25 mA	6.21	1.65

Table 6 Result of the Ra parameter obtained in the different samples

To compare the Ra value between the different samples, each sample was divided into 16 areas (4X4), in each area an average of Ra was taken and compared with the

corresponding area of the other reference sample for the evaluation of the specific parameter.

Figure 31 shows the results obtained, highlighting as for every single area of the 16 sampled, the Ra value is always higher or lower than the corresponding area of the other sample. This gives a confirmation on the influence of each single parameter examined on the roughness.

figure 31a shows that the S1X2 sample with a thickness of 5.5 mm has an average roughness parameter of 4.25 mm while the S1X3 sample with a thickness of 7.5 mm has an average Ra of 9.99. This result confirms that increasing the thickness increases the surface roughness. Similar results can be found in figures 24 b, c, d respectively for current, scan speed and focus offset. Concluding that the Ra value increases with increasing beam current and decreases with increasing scan speed and offset focus.

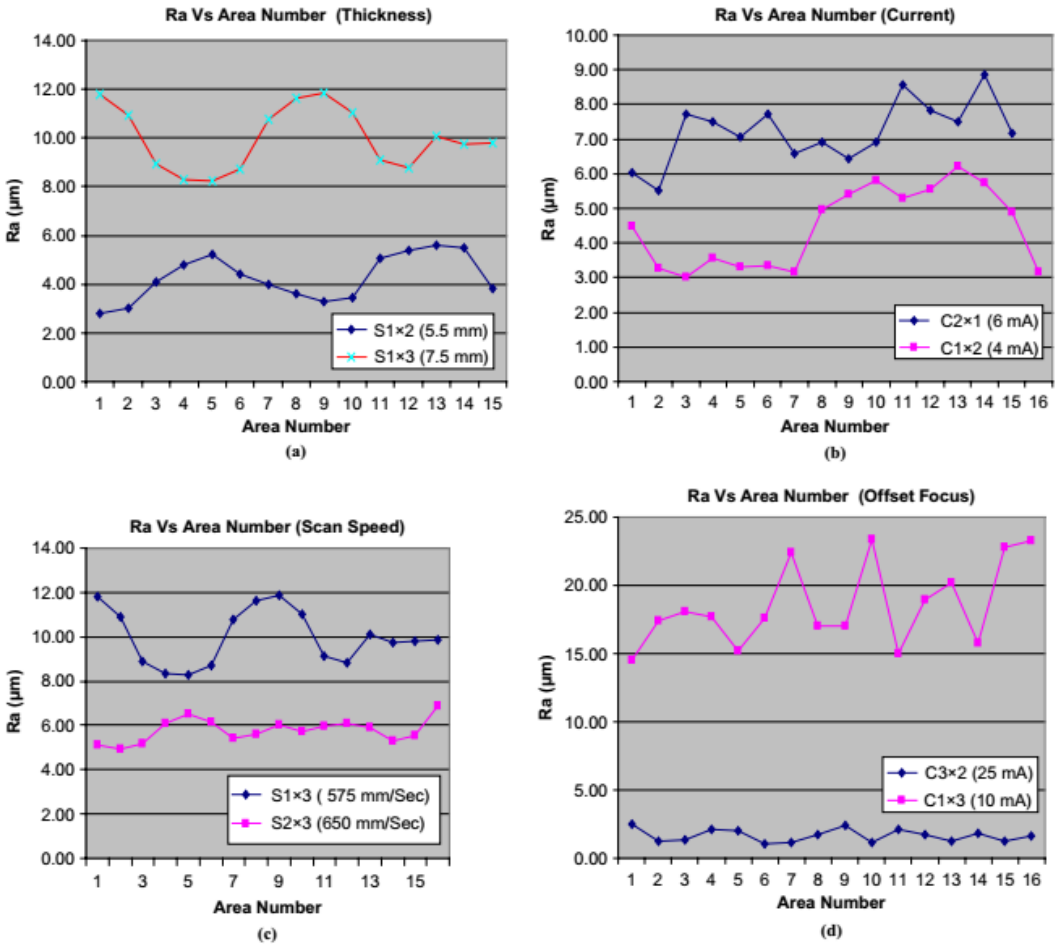

Figure 29 Ra trend in the different samples comparing: Thickness of 5.42 and 7.42 mm; (b) current of 4 and 6 mA; (c) scan speed of 575 and 650 mm / s; (d) offset focus of 10 and 25 mA [19]**.**

All these parameters are related to energy density, concluding that an increase in energy density leads to a rougher surface, in opposition to the problem of porosity.

Finally, the multiple regression equation obtained from the experimental analysis is reported. In general there is a matrix problem of the type eq (8):

$$y = X\beta + e \qquad \text{eq (8)}$$

With "y" the vector of the observed results with dimension qx1, "X" is the matrix of independent variables of size kXq with k the number of times that the experiment was repeated and q the number of independent variables, in this case 4, "β" is the vector containing the coefficients of the independent variables (qx1) and "e" is the vector of random errors (1xk). The estimated equation is eq (9):

$$R_a = 4.85+7.8\ A+4.2B-10.5C-0.5D \qquad \text{eq (9)}$$

The equation provides the surface roughness Ra as a function of the four independent variables A, B, C, D which are sample thickness, beam current, scan speed and focus offset respectively. Figure 31 graphically shows the comparison between the predictive results and the experimental results.

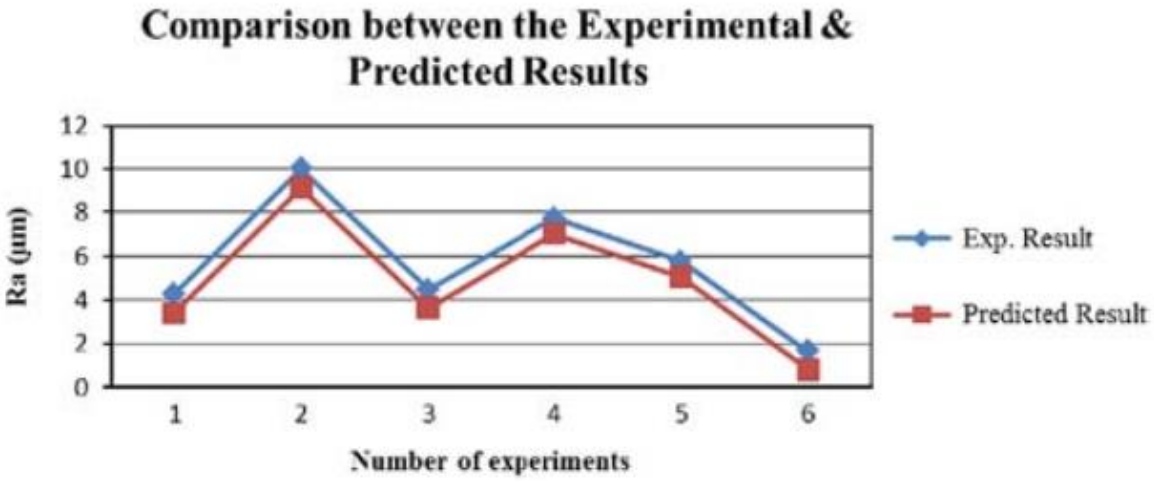

Figura 30 Comparison between predictive results and experimental results.

The model is robust and its adequacy has been verified through ANOVA statistical analysis, also calculating the statistical parameter R^2 which varies between 0 and 1.

the R^2 parameter is an excellent indicator of the reliability of the equation, which will be more suitable for the sample data, as the value R^2approaches 1. The value of the resulting R parameter is 0.997, therefore in statistical language it can be said that: "there is no sufficient reason to reject the proposed equation" [19].

From the analyzes reported, some relevant considerations can be made on the origin of roughness in EBM. One of the important phenomena in roughness is the sintered powder that sticks to the surface of the parts. In general, the amount of powder used in each single layer is much less than available. The melting pool acts as a heat source for this unused powder, and through conductive phenomena sinters it. If the energy of the melting pool increases, the phenomenon is amplified, and the quantity of sintered powder increases, leading to a greater roughness. The relationship between energy density and roughness can be explained by this phenomenon. If there is an increase of the energy density and therefore the energy supplied to the melting pool, for example through a high beam current, a low scanning speed and a low focus offset, there is an increase in surface roughness, with a wavy structure with larger peaks and valleys. In addition, the use of a thicker layer leads to a greater use of energy, with a large accumulation of heat in the part. The sintered powder on the surface will increase, with a further increase in roughness. Finally, it is appropriate to mention the influence of the powder size. The use of a powder with a smaller diameter allows the setting of layers with smaller thicknesses and therefore to obtain a lower roughness. This is another limitation of the EBM process, which can only use powder with diameters greater than 45 microns, due to the pushing phenomenon discussed in paragraph 1.1. This is a reason that makes EBM less performing than SLM in terms of roughness. The SLM technique hasn't limits in the minimum diameter of the powder to be used, and presents a lower step effect and less roughness [20].

4.2 Dimensional accuracy

In the EBM process as well as for all AM processes, many factors influence dimensional accuracy. First of all the phenomenon is already influenced, starting from the CAD model, before the building process. After designing the CAD model of the part to be produced, the software releases a file with STL format, essential for the subsequent reading of the part by the AM machine. In the STL format, the surfaces of the part are approximated by triangles (figure 33). If the surface is approximate with many triangles, the dimensional quality of the part to be produced will be better. However, the file size increases significantly as the number of triangles increases, making it difficult for machine software to process. So given the limitation on the number of triangles, it will be more difficult to correctly approximate the surface of the part. This gives rise to the first cause of dimensional error in the EBM process [21].

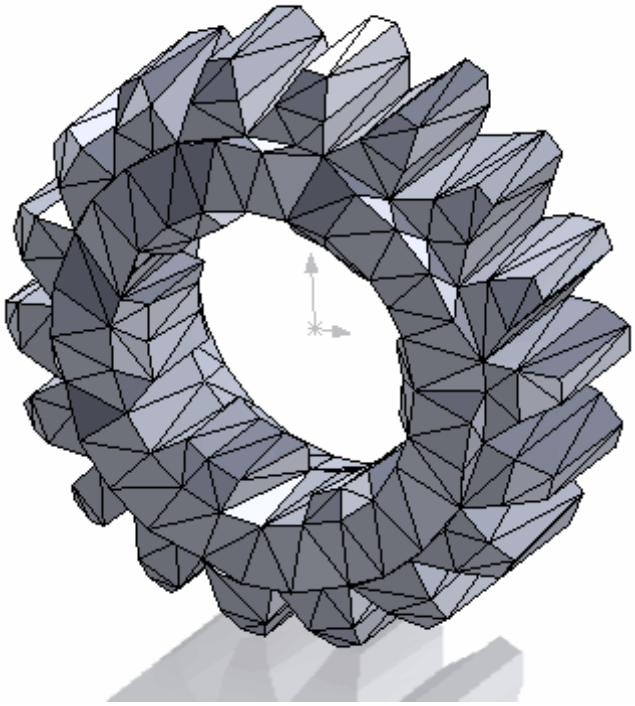

Figure 33 example of a gear wheel model converted to STL format

Furthermore, another factor that could compromise the dimensional quality of the part is the phenomenon of contraction during the solidification process. This contraction may not occur uniformly and create distortions. In addition, the parts with a high thickness can have a high thermal inertia. This can lead to a higher temperature around them, and a greater shrinkage than parts with a lower temperature [21]. To overcome this phenomenon, the sintered powder by preheating each layer and appropriate supports are used, which together can limit this shrinkage and conduct the accumulated heat from the melting pool to the starting plate and the machine structure [22]. The supports must conduct heat but at the same time they must be easy to remove at the end of the process, they are usually designed and optimized automatically by preprocessing software specific for additive manufacturing. An example is the Magics software, also used for the study of this thesis project. Another solution that can be adopted is the application of a scale factor in the STL file, along the X, Y, Z axes of the chamber. To give a quantification of how much the phenomenon of deformation can be relevant, the study by B. Vayre et al is reported [22]. In this study, they tried to quantify how much the deformation of a Ti-6Al-4V plate 1 mm thick could be, in function of the supports. The experiment was carried out by positioning the plate parallel to the start plate of the machine (where the phenomenon shows the maximum deformation) at a distance of 5 mm from it. They chose 5 mm as the distance, since from a distance between 0.05 - 0.10 mm from the start plate no deformation is observed, while with a distance between 5 mm and 15 mm the deformations are similar. However, studying the range from 0.10 mm to 5 mm, the distance of 5 mm shows the maximum deformation. As supports, they chose cylindrical structures with a diameter of 0.6 mm, easy to remove. They conducted several experiments by positioning these cylinders along the perimeter and under the plate. The difference of each experiment was in the number of supports used (and therefore the support density). In total they tried seven sets of supports, with a respective distance between the cylinders of 2, 3, 4, 6, 8, 10 and 12 mm respectively.

Figure 33 shows the scan of the plate, obtained by means of an optical sensor, with the supports placed every 12 mm.

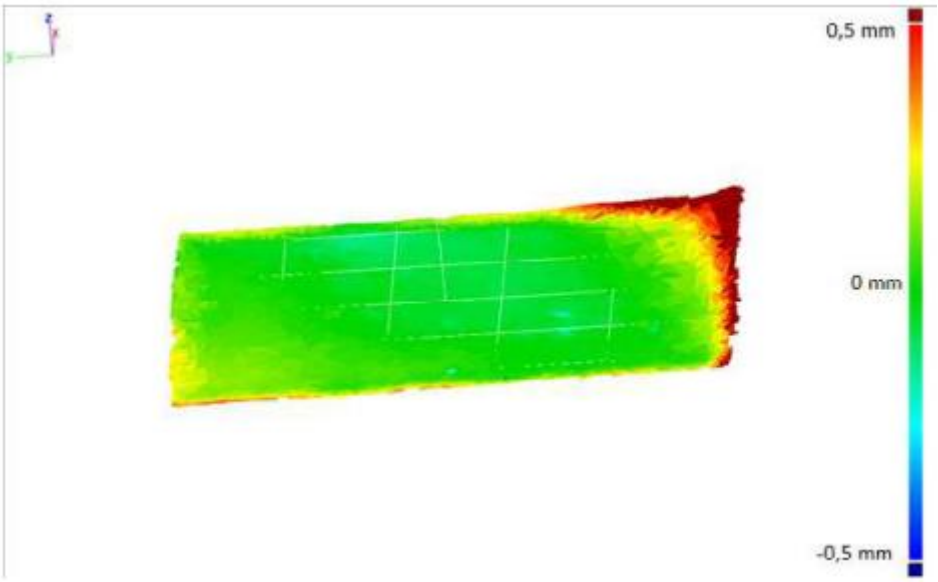

Figure 33 scan of the plate, with the supports placed every 12 mm [22]

As can be seen from Figure 33, the support density has a high influence on the surface flatness. The maximum deformation is observed in the boundary of the plate, where the deformation can exceed 0.5 mm in height. For completeness, the standard deviations of the plate points are shown for each set of supports (figure 34).

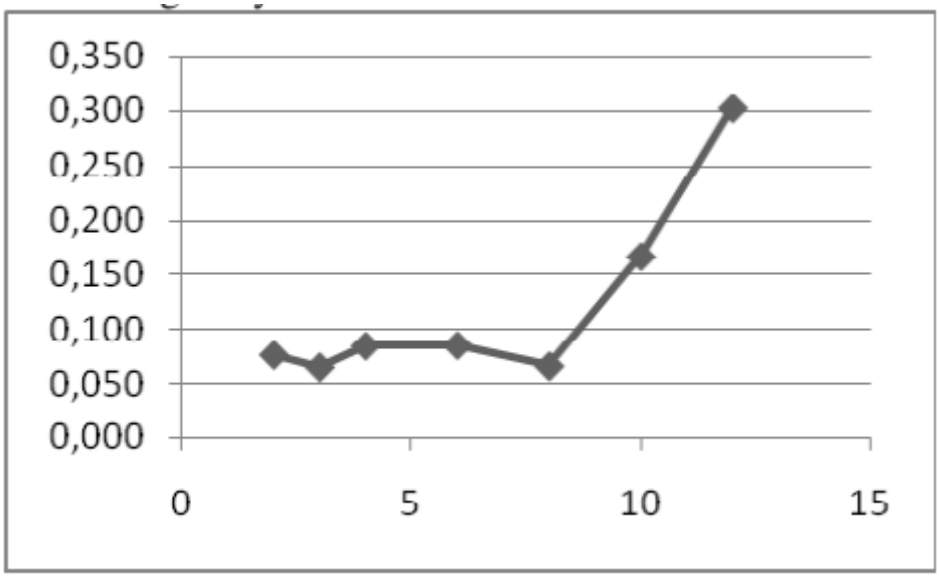

Figure 34 the standard deviations of the plate points, in function of the distance between the supports [22]

Figure 34 shows how the best set of supports for minimizing deformation is the set with a space between the cylinders of 8 mm. Furthermore, the choice of 8 mm set, also optimizes the material lost by the supports choosing the minimum required, in contrast to the pre-procesing software that would use the spacing of 2 mm. This is just a simplified example of the shrinkage phenomenon, having analyzed a simple plate with a thickness of 1 mm. In the construction of pieces with higher thicknesses and more complex geometry, where there is the need to dissipate a greater quantity of energy, a much more accurate analysis about the quantity of supports and their optimization will be required.

Other phenomena that can influence the dimensional quality of the part are the orientation and position in the building chamber of the part. In this regard, it is useful to analyze the experiment conducted by Franchitti et al [21]. The experiment consists in the evaluation of the dimensional repeatability in the EBM process and which of the factors between orientation, position of the part in the XY plane and position in height along the Z axis of construction can influence the quality of the product.

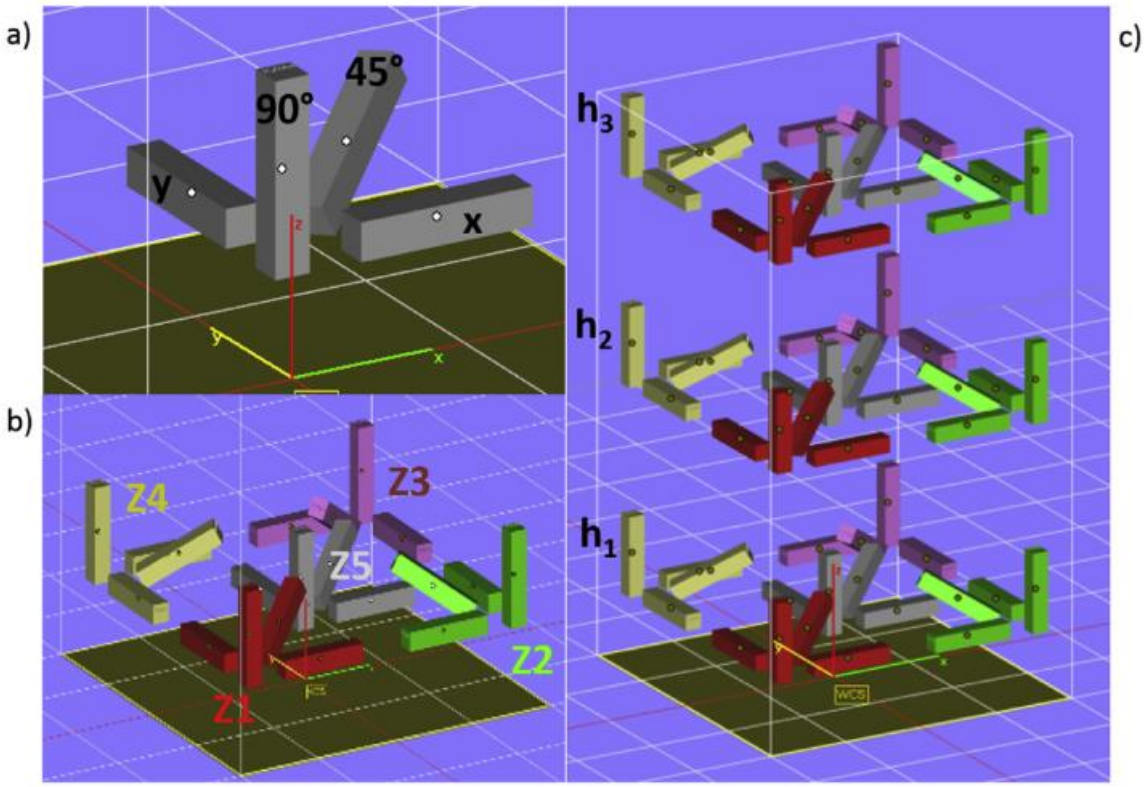

Figure 34 Set of samples built for the experiment: (a) set of samples to evaluate the orientation; (b) set of samples to evaluate the position in the XY plane; (c) set of samples for the height position [21].

To understand which of the phenomena mentioned was relevant, they built a set of four rectangular samples, with different orientations, and specifically parallel to the X, Y, Z axis and one inclined 45 degrees respect to the XY plane (figure 34a). This set of specimens was replicated five times in the XY plane to evaluate the effect on the positioning in this plane (figure 34b), and the entire set built in the XY plane was replicated three more times in height to evaluate the effect on the positioning in the Z axis of construction (figure 34c). The material is the Ti6Al4V and all the samples were produced with a layer of 50 µm. To evaluate dimensional repeatability, the experiment was repeated twice. The variable taken into consideration is the thickness of the square base sample equal to a nominal size of 10 mm. The statistical analyzes

conducted by Franchitti et al, have shown that the EBM technique has good repeatability. Table 7 shows the global results of the repeated experiment.

	Mean Average thickness [mm]	Standard Deviation [mm]	Min Value [mm]	Max Value [mm]
RUN 1	10.000 ± 0.138(3σ)	0.046	9.862	10.080
RUN 2	9.995 ± 0.141(3σ)	0.047	9.862	10.101

Table 7 statistical results of the repeated experiment [21].

Furthermore, the results correspond to the precision declared by Arcam for the EBM process equal to 0.13 mm with a confidence limit 3σ, for a length of 10 mm.

The analysis also revealed that the inclination and positioning of the piece on the construction chamber have a significant influence. From table 8 which shows the global ANOVA of all the data, and from the interaction plot in figure 35, it is clear that the two factors that influence the most, are the inclination and positioning of the piece on the XY plane that with their interaction explains 95% of the thickness variance. Even the height along Z has its influence, but its relevance is much less than the other two factors.

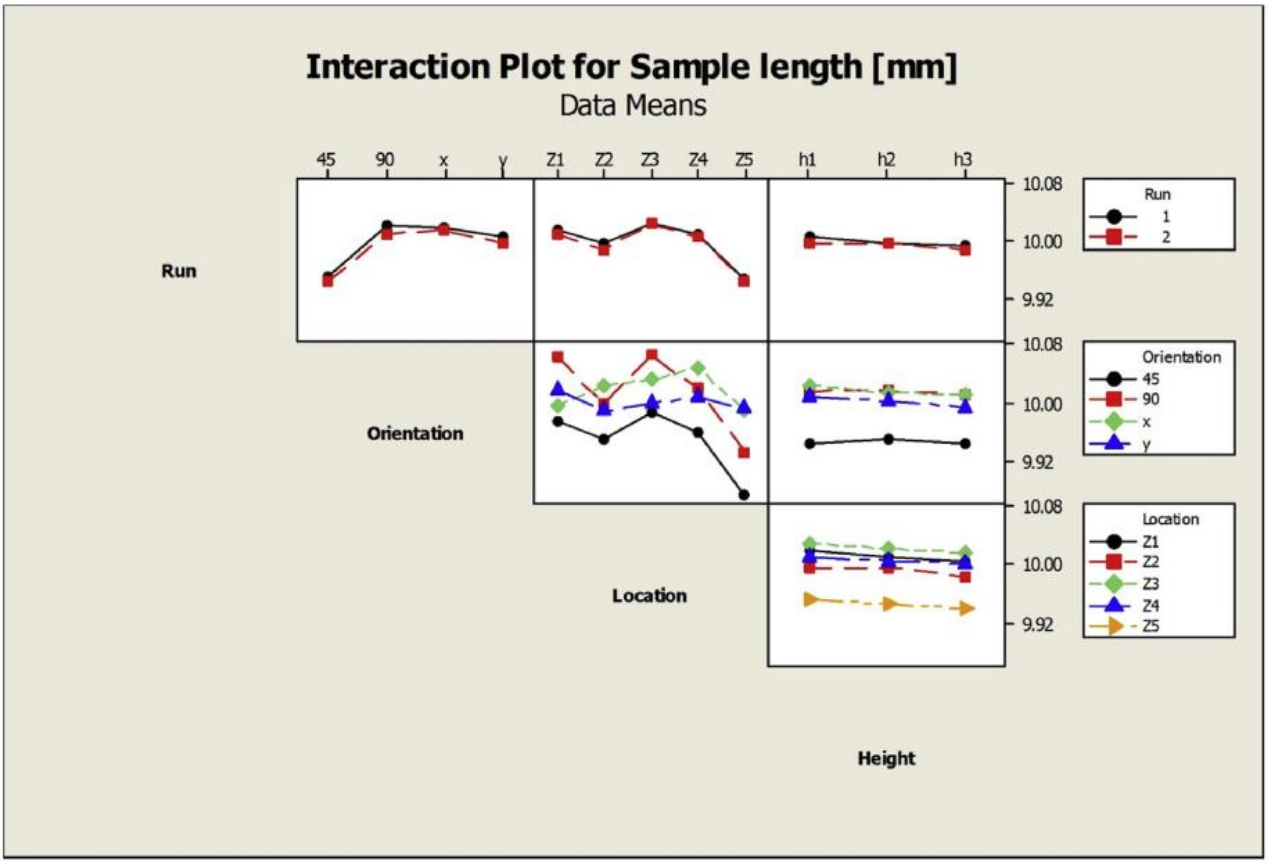

Figure 35

Source	DF	Seq SS	Adj SS	Adj MS	F	P
orientation	3	0.096178	0.096178	0.032059	252.11	0.000
location	4	0.087422	0.087422	0.021856	171.87	0.000
orientation*location	12	0.055611	0.055611	0.004634	36.44	0.000
height	2	0.002988	0.002988	0.004940	11.75	0.000
Error	98	0.012462	0.012462	0.000127		
Total	119	0.254661				
R-sq	95.11%					

Table 8 Global Anova of the two repeated experiments

By observing the interaction plot from figure 7 it can be observed that the samples with the smallest thickness are the set positioned in the center of the construction chamber (zone 5). This phenomenon is caused by thermal contractions, due to the different thermal inertia and the different heat exchange that occurs in the central area, between the parts during the solidification process. A possible solution would

be to set dynamic scale factors as a function of thermal inertia instead of a constant scale factor suggested by Arcam. The constant scale factor also affects pieces inclined 45 degrees. In fact, these pieces, like the pieces positioned in the center of the chamber, are those with the least thickness. The 45-degree inclined pieces are the only ones affected by the Z scale factor, while the remaining pieces are influenced only by the X and Y scale factors. This suggests that a constant Z scale is unsuitable. As already mentioned, the positioning of the part in height along the Z axis has a lesser effect than the positioning in the X-Y plane and the inclination of the piece. However, the analyzes showed thicknesses slightly lower as the height of the chamber increased. Also in this case, the cause is attributable to an uneven shrinkage and to the use of a constant scale factor.

List the main problems and causes of the dimensional quality of the EBM process, in the next paragraphs, the last aspect that can influence the dimensional quality of the product, the melting strategy, will be discussed. From the studies reported, it has been seen that the main problem of dimensional quality is heat management. The right melting strategy can influence heat distribution in a positive way. The main purpose of this thesis is to verify that the contour strategies associated with the MultiBeam technique can improve the dimensional and geometric quality of the EBM process.

4.2.1 The effect of contour strategies on dimensional quality

As already mentioned in the previous paragraphs, the contouring strategies and specifically the use of the MultiBeam, has a significant influence on the quality of the product. This strategy, maintains active different melt pools simultaneously, moving the beam quickly. By activating multiple melting pools rapidly and simultaneously, there is an optimization of the thermal gradients, that influence the temperature distribution inside and around the melting pool. The melt pools are small and a rapid solidification takes place. This allows to “freeze” the geometrical contour of the part, resulting an improved quality in terms of dimensional and geometrical tolerances.

However, only little research is available for contour strategies in EBM. The analyzes carried out at the IAM laboratory of the Polytechnic of Turin with the collaboration of the company ASF METROLOGY, have been finalized, to give a systematic view on the effect of this strategy. To quantitatively evaluate the performance and accuracy of EBM with the contour strategy, the benchmarking procedure was adopted. The benchmark is provided to give a systematic process for assessing the validity of organization, products, services, machines and processes by comparing different similar systems, and in this case it was used to evaluate the performance of two different similar processes. It is a consolidated procedure in research, since the first rapid prototyping (RP) systems in the late 1980s, due to the lack of an international reference standard for the quantitative evaluation of the performance of these machines [23]. Having to evaluate the dimensional accuracy and tolerances of the parts produced, it is useful to use the ISO standard IT grades, in order to systematically summarize the accuracy of the process.

4.2.2 Benchmark

To evaluate the influence of the Contour on dimensional accuracy, two different types of materials were compared, TiAl and Ti64, building four identical pieces respectively, two for each material. For each pair of pieces, the same process parameters were maintained, with the difference that in one of the two pairs the contour strategy was activated while in the other piece it was deactivated. The piece was built with reference made by Moylan et al, for a correct benchmark including a higher number of features with respective as many dimensions for each basic sizes range. The indications are as follows [23]:

- have a significant number of features with small, medium and large sizes;
- do not use high quantity of material;
- have many features of functional parts ;
- Use simple geometries, so that it is easy to measure and define them;
- make sure that the measurements are easy to repeat;
- make sure that there is no need for post-treatments or manual interventions such as support structures ;

The measurements of the replicas of the two different processes for the two materials were carried out through a Coordinate Measuring Machine (CMM), and subsequently reworked in terms of IT grades associated with the dimensions of the ISO base respect to the tolerances and geometric characteristics of the reference part.

4.2.3 The reference part

The benchmark reference (figure 32) was designed following the indications given by Moylan et al, cited in the previous paragraph. There aren't supports and It consists mainly of simple classic geometries (cylinders, spheres, planes and cones), in both concave and convex forms, to consider different design possibilities. Classic geometries were chosen, since the evaluation of geometric tolerances and shape errors is based on them.

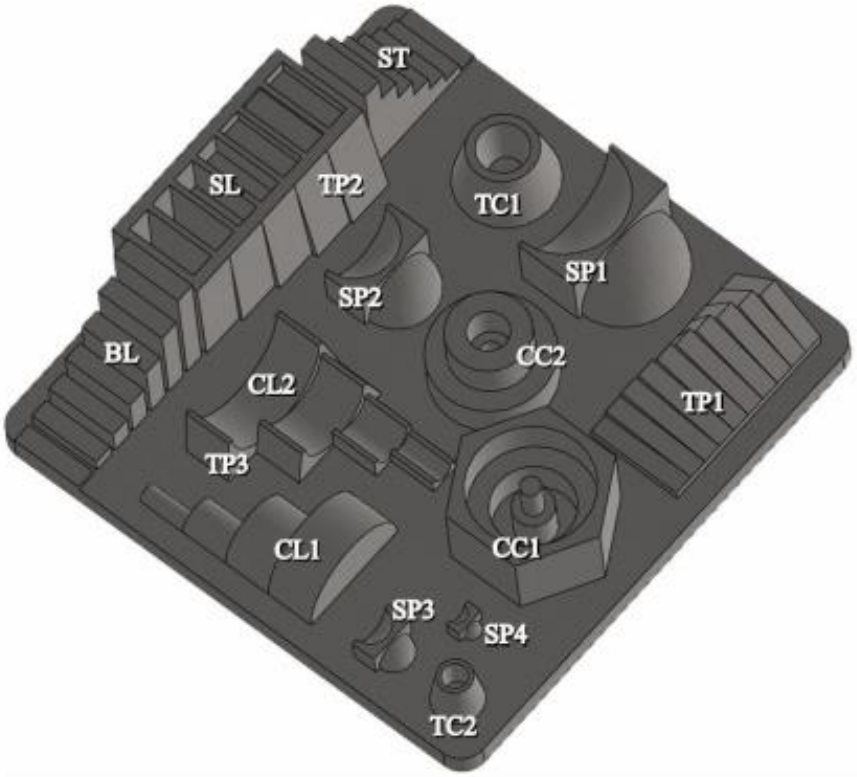

Figure 31 CAD model and geometries of the reference part.

As can be seen from this reference, there are similar geometries with different sizes, In order to test different ISO range 1 -3 mm, 3 - 6 mm, 6 -10 mm, 10 - 18 mm, 18 -30 mm, 30 - 50 mm, 50 - 80 mm, 80 -120 mm. The geometries were built on a 5 mm thick square plate, this thickness was chosen to prevent deformation of the piece during manufacture. Furthermore, the geometries have been positioned and oriented in

order to make the measurements easy. The reference taken into consideration, is similar to the reference designed in benchmark study presented in another article [23] by the research group of P. Minetola, L. Iuliano, G. Marchiandi used to make assessments on the geometric and dimensional tolerances of additive manufacturing processes, validated for polymeric processes such as Fused Deposition Modeling (FDM).

The reference consists of the following geometries:

- *seven rectangular blocks (BL):* all the blocks are separate and have a base of 4 mm x 15 mm with a height that varies according to the sequence: 1 mm-3 mm-6 mm-10 mm-15 mm-21 mm-28 mm.
- *Seven rectangular slots (SL*): the slots are embedded in a rectangular block with a high of 28 mm, and each slot has a base of 5 mm x 15mm with a depth ranging from 1mm to 28 mm with an identical sequence to the BL blocks.
- *seven steps (ST):* the steps are joined together and form a staircase, with a height ranging from 28 mm to 1 mm with the same height as the BL blocks but with an inverse sequence.
- *one pair of coaxial truncated cones (TC1):* they consists of a concave and a convex cone, both truncated. In the set, the outer cone has a major diameter of 22 mm and a minor diameter of 13.6 with a height of 12 mm. The internal cone, on the other hand, has a major diameter of 10 mm and a minor diameter of 6.5 mm.
- *a set of coaxial cylinders (CC2):* the CC2 set consists of two cylinders with diameters of 3 mm and 16 mm and two blind holes with a diameter of 8 mm and 24 mm, all features have a height of 8 mm.

- *two sets of quarter spheres (SP1, SP2):* each set consists of a quarter of a concave sphere and a quarter of a convex sphere with the same dimensions. The diameter of each set is 16mm and 24mm for SP1 and SP2 respectively.
- *a serieof inclined planes (TP2):* The series of planes TP2 is located on the vertical face of the SL block. The inclination of the planes, with respect to the vertical plane, varies with the sequence 0-2 -4.5-7- 9 degrees. The TP2 series was conceived to study the effect of inclinations lower than 5 degrees
- In addition, other orthogonal planes or parallel to the reference base were built.

In total there are more than eighty features to be evaluated, which allow over a thousand measurements between dimensions and distances in the ISO range, which varies from 1 mm to 120 mm. In addition, the banchmark and the arrangement of the pieces has been designed to be able to take all the measurements using a single configuration of the CMM probe with the axis orthogonal to the base plane, with a probe diameter of 2mm, since there is enough space between the features.

4.2.4 Production and inspection

the reference parts were produced with the Arcam EBM A2X machine (figure 34), with a working chamber of 200 x 200 x 380 mm (x, y, z), a maximum power of 3 kW and a

temperature range between 600-1100 C° [24]. The powder used to build the four reference parts are TiAl and Ti64, with a minimum diameter of 45 microns.

Figure 34 illustrative image of the EBM A2X machine [24].

Four reference parts were built, two for each material with Contour active and inactive. Due the limitation of the chamber size and to avoid deformations caused by

the excessive thermal inertia of the base plate, the benchmarks of the two different processes (with and without Contour) have been divided into four parts (figure 32). In addition subdividing references avoids the problem of having a strong material difference between one layer and another that could lead to the melting pool problems.

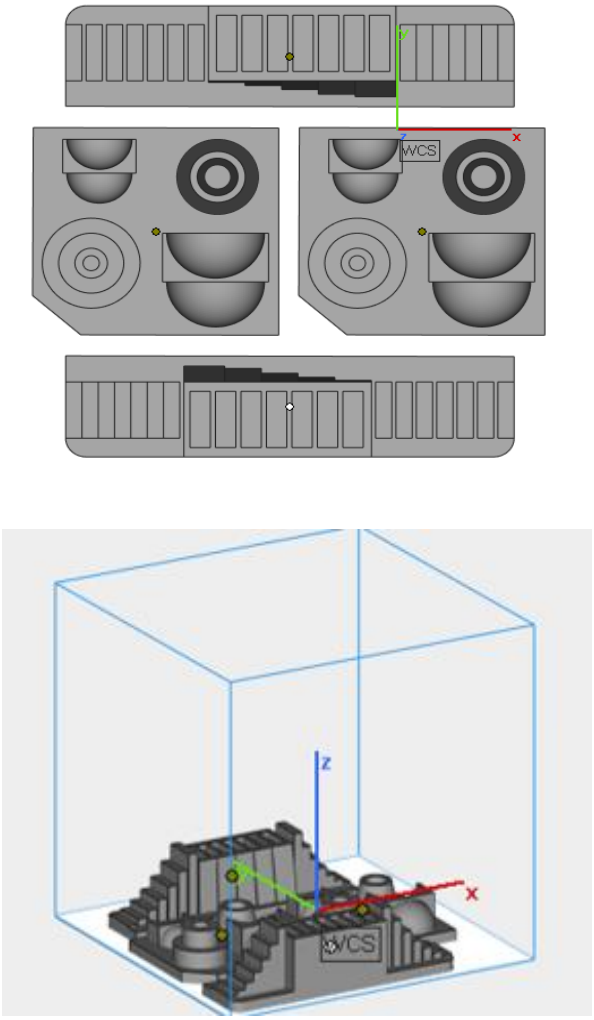

Figura 32 position of the four parts of the corresponding material in the build chamber

The reference parts after production were freed from the breakaway powder, using the sandblasting process with the same powder used in the construction process.

Each replica, after construction, has not been post-processed and has not undergone any surface alteration effect. The reference parts were inspected using the CMM machine Altera S, present in the ASF Metrology laboratory (figure 33).

Figura 33 CMM Altera S used to make measurements.

The measuring machine has an MPEE (Maximum Permissible Error) of 1.8 µm + L/400. Each measurement was performed three times, and its average was taken as the value for the analyzes.

4.2.5 Results of dimensional inspection

The measures obtained through CMM have been elaborated to evaluate the dimensional accuracy of the two processes in terms of IT ISO grades. The tolerance values range from IT 5 to IT 18 and have been evaluated for nominal dimensions up to 500 mm, using the standard tolerance factor *i*, expressed in micrometers with eq (10):

$$i = 0.45 \cdot 3\sqrt[3]{D} + 0.001 \cdot D \qquad \text{eq (10)}$$

With D equal to the geometric mean of the extremes of the iso range, where the dimension to be measured falls. (table 11) eq (11):

$$D = \sqrt{D_1 \cdot D_2} \qquad \text{eq (11)}$$

Range		**Basic sizes**							
Above	D_1 (mm)	1	3	6	10	18	30	50	80
Up to and including	D_2 (mm)	3	6	10	18	30	50	80	120
Standard tolerance factor	i (μm)	0.542	0.733	0.898	1.083	1.307	1.561	1.856	2.173

Table 11 range of basic size and corresponding tolerance I [25]

The corresponding IT grades of the measurement is calculated as the number of times *n* that the tolerance i fits in the dimensional deviation [25] eq (12):

$$n = 1000 \cdot \frac{|D_n - D_m|}{i} \qquad \text{eq (12)}$$

Where D_n and D_m correspond respectively to the nominal dimension and the measured dimension of the feature.

Table 12 illustrates the corresponding IT grade of the measure according to the value *n*. When the value *n* found is between two IT degrees, it means that the machine for that particular measure is not able to provide the lowest value between the two

degrees and the IT degree immediately higher is assigned [25]. For example, for an *n* equal to 700 it corresponds to IT 16 rather than an IT 15.

Basic size		Standard tolerance grades													
Above	Up to	IT 5	IT 6	IT 7	IT 8	IT 9	IT 10	IT 11	IT 12	IT 13	IT 14	IT 15	IT 16	IT 17	IT 18
1 mm	500 mm	7*i*	10*i*	16*i*	25*i*	40*i*	64*i*	100*i*	160*i*	250*i*	400*i*	640*i*	1000*i*	1600*i*	2500*i*

Table 12 Classification of IT grades according to ISO 286-1:1988 [25]

In summary, for the measurements, a distribution of n is obtained for each ISO range, for the two process. For each distribution in the corresponding ISO range, the 95th percentile is taken as the maximum dimensional error of the EBM machine to evaluate the accuracy through IT degrees in line with previous studies in the literature. The results of the analyzes carried, are shown in figures 33 and 34, where through a bar chart, the dimensional accuracy of the two different processes (with or without the Contour), for each ISO range is indicated for the corresponding TiAl and TI64 materials.

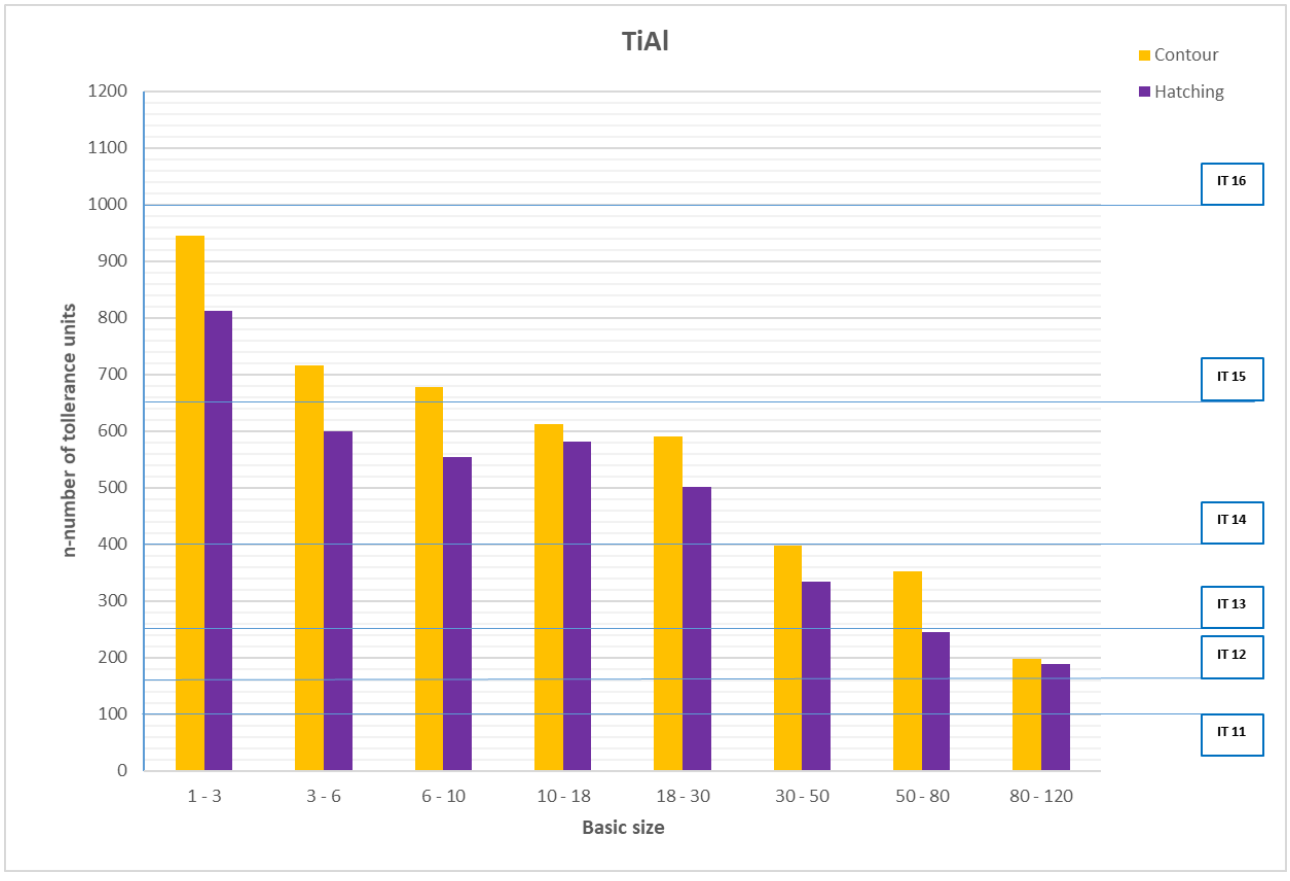

Figure 34 Dimensional accuracy (95th percentile) of the two processes EBM TIAl and TiAl with Contour compares in terms of IT degrees for different ranges of ISO base dimensions.

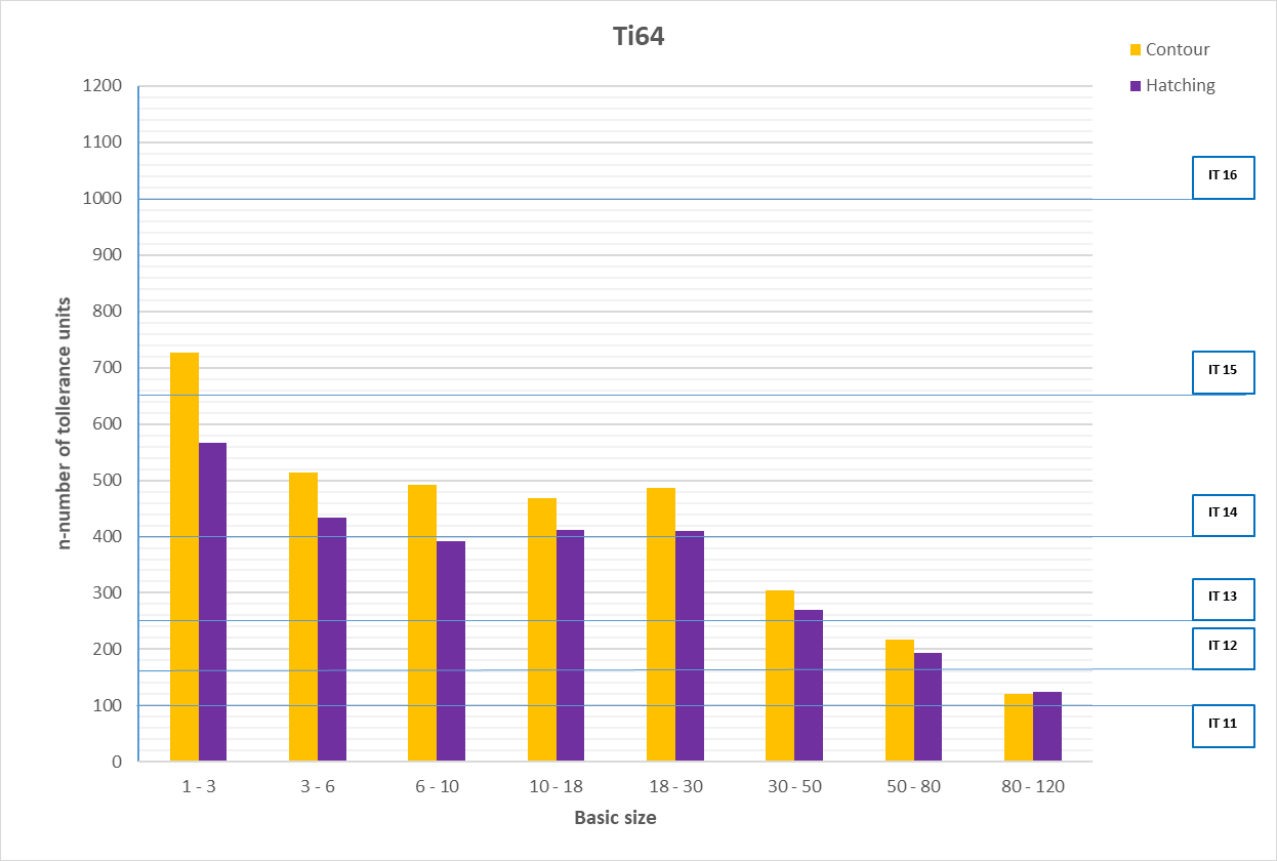

Figure 35 Dimensional accuracy (95th percentile) of the two processes EBM Ti64 and Ti64 MB with Contour compares in terms of IT degrees for different ranges of ISO base dimensions.

The graphs show that the artefact in which the contour is realized has a lower dimensional accuracy. In all IT bases the number n is higher for the TiAl with contour than the TiAl without contour, although for most of the IT bases, from the base 10-18 mm to the base 80-120 mm they slightly maintain the same IT grade. The IT grade for the part manufactured with TiAl and using a contouring strategy process varies from IT16 (for the smaller size) to IT13 (for the larger size). In any case, the quality of the process, in each ISO range, is worse or at least equal to the corresponding process without contour. Regarding the IT quality of the TiAl process without contour it varies from IT 16 to IT13 for larger basic dimensions, with an improvement of the IT grade for bases 3-6mm and 6-10 mm.

A similar worsening effect can also be seen for Ti64 with contour respect the Ti64 without contour, although in comparison to TiAl, as a material, it reports an improvement on IT grade. The IT grade for the part manufactured with Ti64 and using a contouring strategy process varies from IT16 (for the smaller size) to IT12 (for the larger size). While the It grade for the artifact made with Ti64 without contour varies from IT15 to IT12 for larger basic dimensions.

The cause can be attributed to the fact that the contour technique creates a perimeter boundary and generate an extra material on the external part and increases the IT grade.

The comparison between the two materials shows that the material is a relevant factor in determining the quality of the process. The parts with the two different materials were not produced with the same process parameters. The process parameters for TiAl have been developed in IAM with the focus to obtain a certain microstructure (gamma phase) and microstructure homogenization rather than optimizing the dimensional quality. This is mainly due to the sensistivity of intermetallic alloys such as TiAl for which even a temperature gradient equal to 20 ° C can strongly influence the final microstructure. For the Ti64 the microstructure is more stable and therefore a wider process windows is allowed also for dimensional quality optimization.

In order to further investigate the dimensional quality, the distances and diameters of the single geometries (spheres and cylinders) were analyzed separately. As confirmed by the previous analysis in terms of distances, the feature of the artifact produced without contour is better than the corresponding ones produced with contour. As regards the geometries, only the internal spheres and cylinders have a better results in the case that the contour strategy is used. The reason for the improvement of these sizes is due to the fact that the contour creates an extra perimeter thickness which leads to a lower deviation respect to the nominal size of

the geometry. Conversely, for the outer spheres, this additional material increase the deviation from the nominal size.

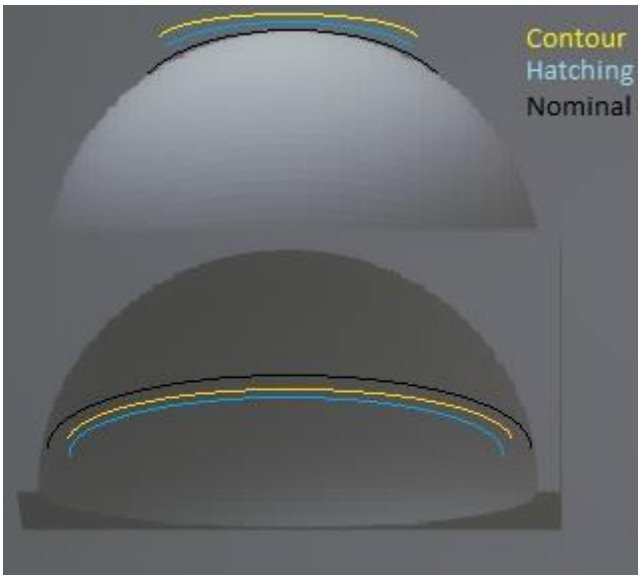

Figure 36 process of melting of the inner and outer sphere with Hatching and Contour respect to the nominal dimension

4.2.6 Results of GD&T inspection

Having established that the contour strategy does not lead to an improvement in dimensional quality, we wanted to investigate the effects of this strategy for geometric tolerances.

For the GD&T the following was assessed:

- flatness: separately for horizontal, vertical and inclined planes, in order to evaluate the effects for each single building direction.
- Parallelism: always separately between the horizontal and vertical planes.
- Perpendicularity
- Coaxiality
- Cylindricity
- The angle of the inclined planes.

The contour has a beneficial effect for the flatness in TiAl, as can be seen in figure 37. The improvement occurred both in the median and interquartile, presenting much smaller blocks. This effect is much more pronounced on the vertical and oblique flatness, where the contour plays a more important role as it acts on the perimeter of the piece.

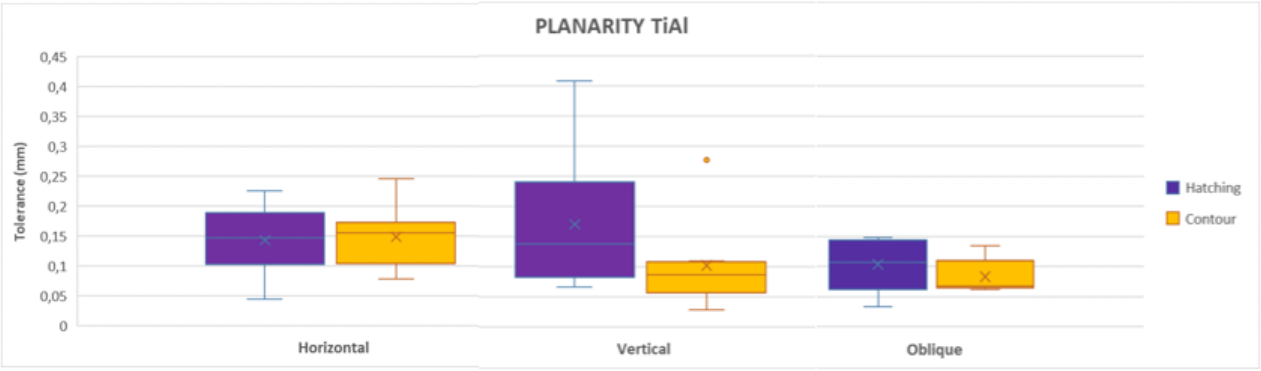

Figura 37 flatness tolerances for TiAl with and without contour in the horizontal, vertical and inclined planes.

A similar effect is found in the case of Ti64, except for the horizontal flatness, where it seems that the contour does not have a beneficial effect (figure 38).

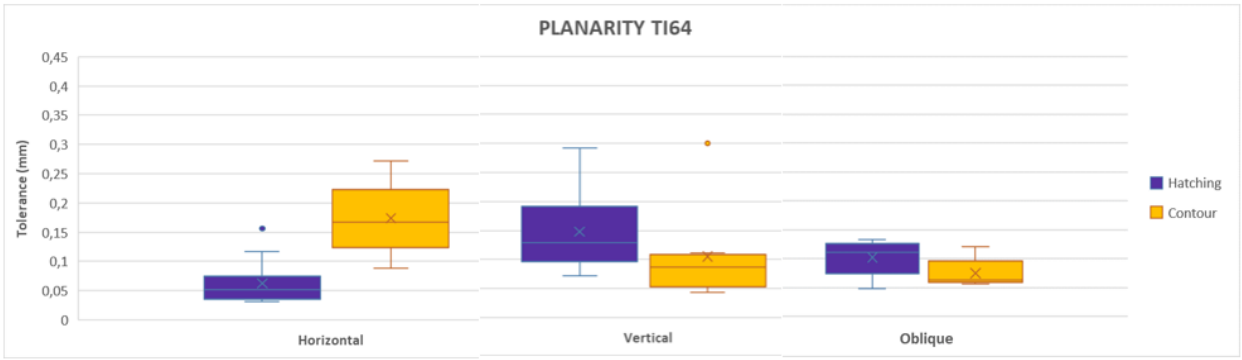

Figura 38 flatness tolerances for Ti64 with and without contour in the horizontal, vertical and inclined planes.

Probably the pejorative effect compared to the case of TiAl is due to the material and the melting process. Ti64 has much lower and variable temperatures (≈ 700 ° C) compared to TiAl (≈1000 ° C), which instead has slower cooling.

This result can be also observed in the case of parallelism (figure 39). Both the vertical and horizontal parallelisms present an improvement for TiAl with contour compared to TiAl without contour (especially for the vertical part). As regards the horizontal parallelism of Ti64 with contour similar to its horizontal flatness, it presents a worsening compared to Ti64 without contour, on the other hand, the vertical parallelism improves.

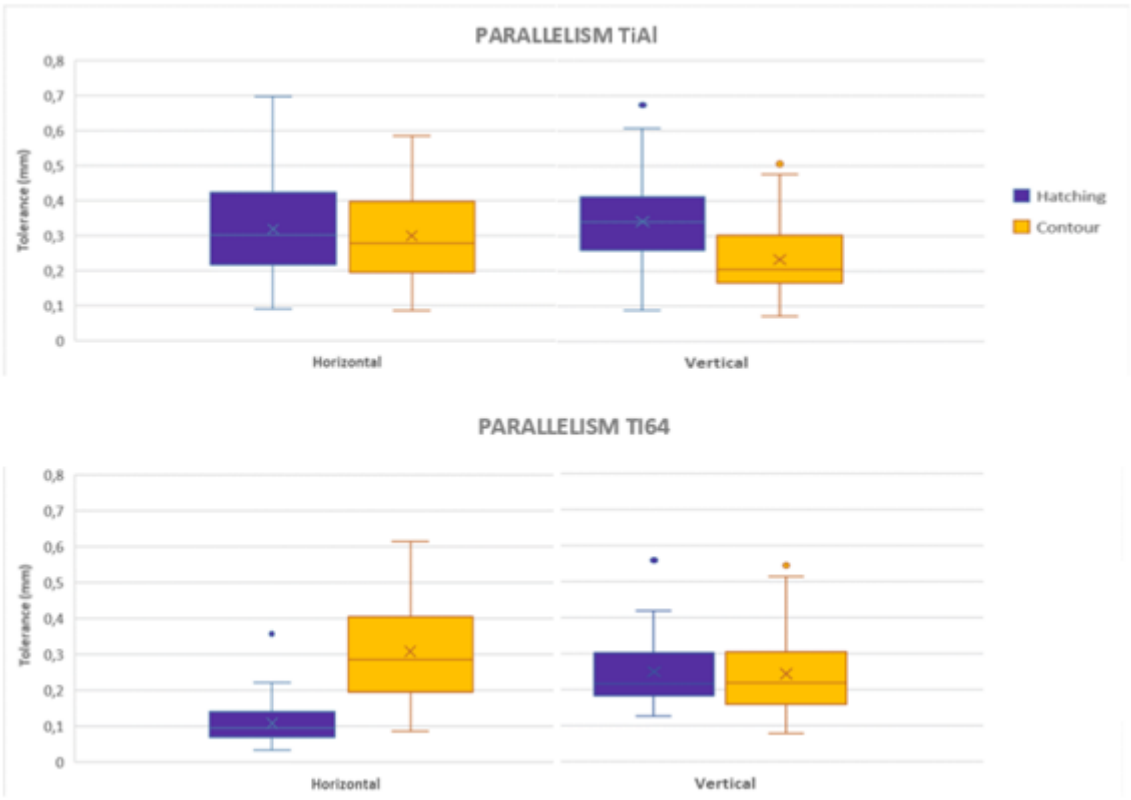

Figure 39 Comparison between vertical and horizontal parallelisms of TiAl and Ti64 with and without contour

As regards the remaining tolerances of perpendicularity, coaxiality and cylindricality, there is an improvement using the contour strategy for both TiAl and Ti64. For these tolerances the contour strategy is therefore effective. The figures below 40,41 ,42 show the results obtained for both materials and for both melting strategies.

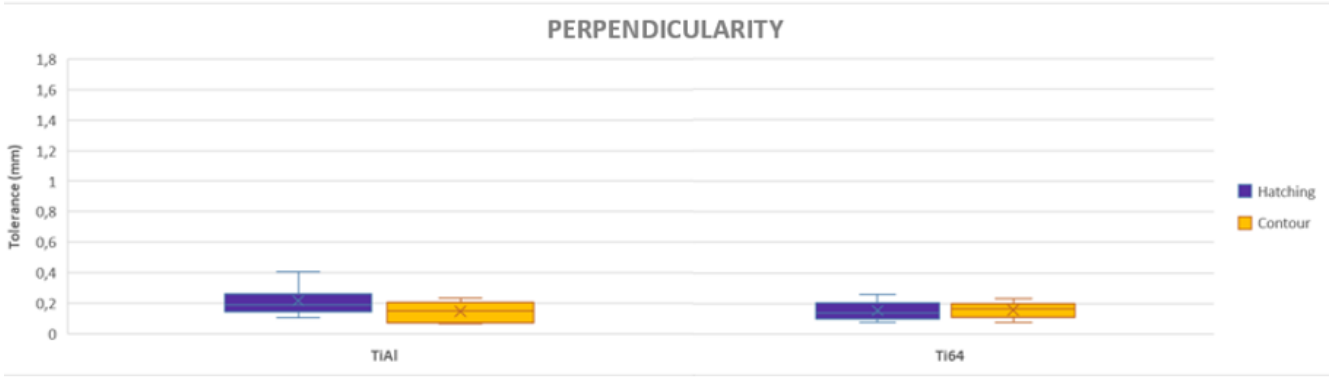

Figure 40 Comparison between perpendicularity of TiAl and Ti64 with and without contour

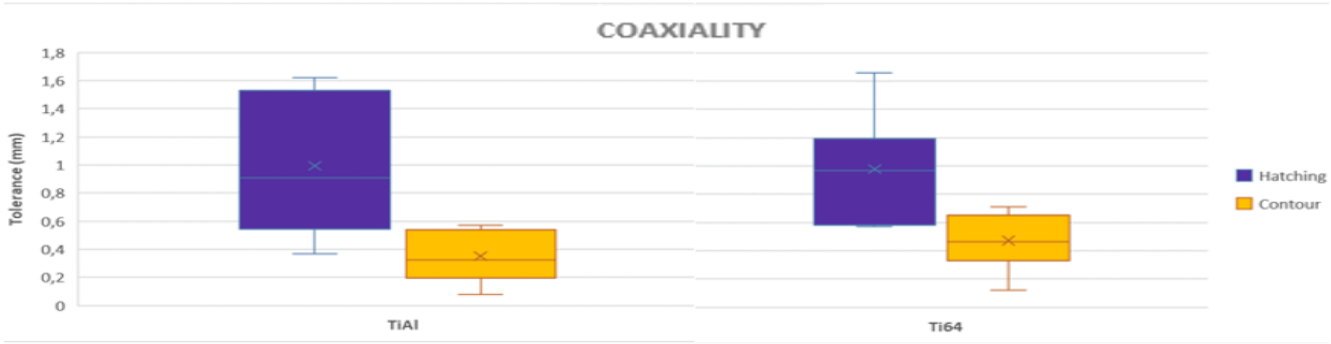

Figure 41 Comparison between coaxiality of TiAl and Ti64 with and without contour

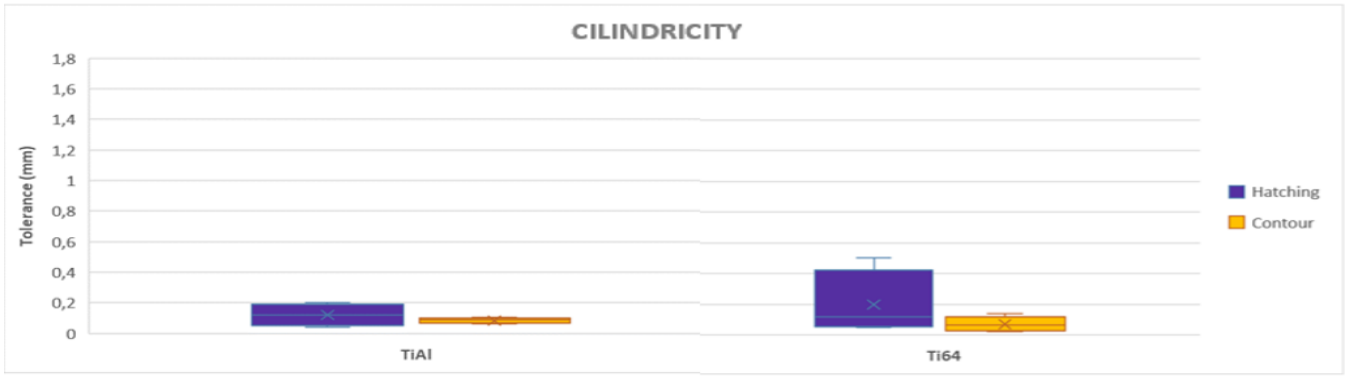

Figure 42 Comparison between cilinfricity of TiAl and Ti6 with and without contour

The contour strategy has also a beneficial effect on the staircase effect. The staircase effect is a consequence of the layer by layer strategy and is typical of all additive manufacturing processes, especially where thicker layer thickness are used [26]. Due to the deposition of the layers on top of each other, steps are created on the inclined surfaces. Figure 43 shows this effect.

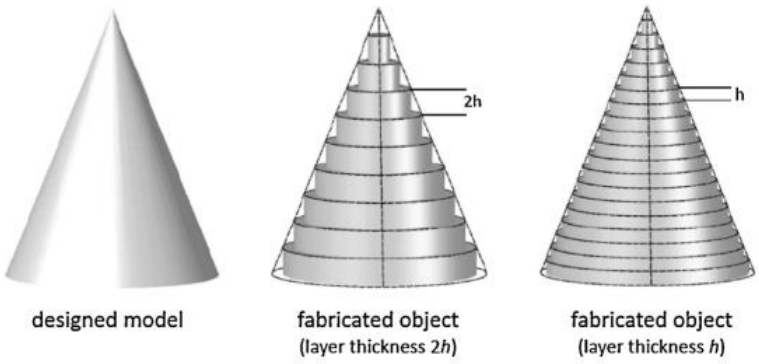

Figure 43 Staircase effect as the layer thickness varies [26].

In both materials, analyzing the angles of the inclined planes, it was found that the staircase effect is less appreciable in the artefacts produced using the contour strategy. A notable improvement in the inclination in all axes, X, Y and Z axes has been observed. Note the different deviation for the two materials, with a better quality for Ti64 than TiAl. This difference can be attributed to the layer thickness. In fact, TiAl artefatc has been produced with a thicker layer (90 µm) respect to Ti64 (50 µm).

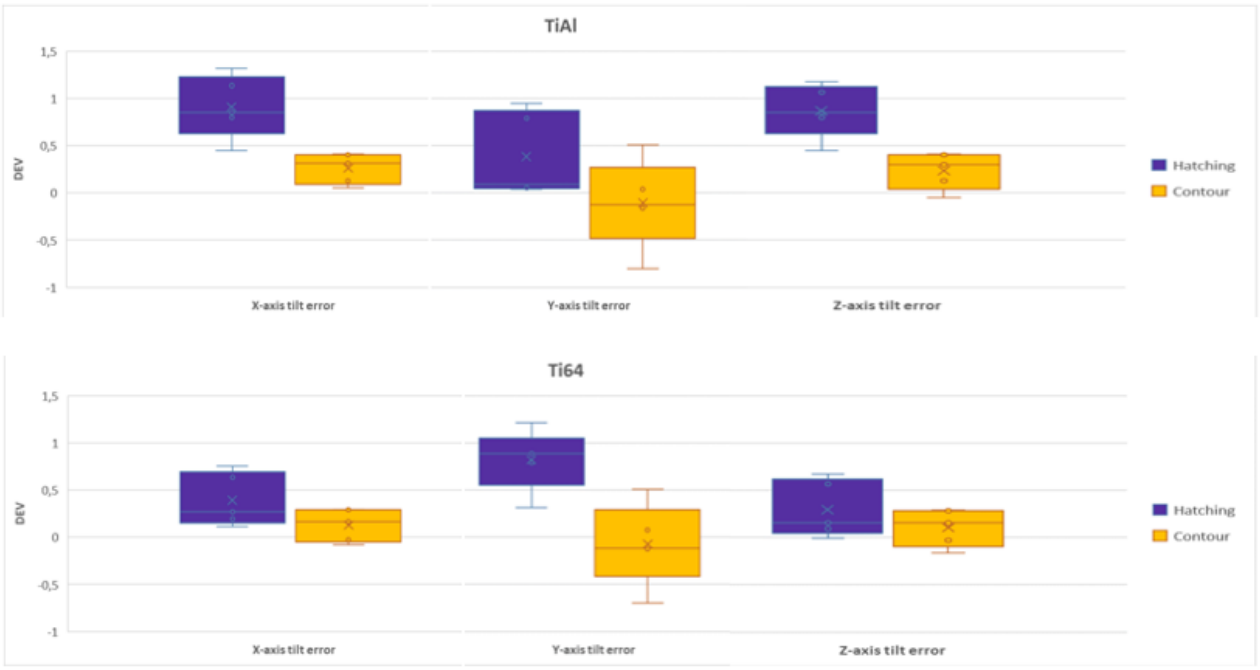

Figure 43 Comparison of the angle deviation for the X, Y and Z axes of TiAl and Ti64 with and without contour

CONCLUSION

In the present thesis work the Electron Beam Melting (EBM) technique has been thoroughly analyzed, specifically the effect that the different melting strategies can bring to the dimensional and geometric quality of the pieces produced has been analyzed. First of all, a thorough literature search was carried out to identify the process parameters that influence this aspect. From the research it appeared that there is no exhaustive knowledge on this aspect. The purpose of the thesis was to fill this gap, addressing a systematic study on the relationship between the different melting strategies and the quality of the piece produced. Specifically, the effect of two different melting strategies was analyzed, the standard strategy which consist of a hatching and contour and the strategy in which the contour has been removed (only hatching) . These strategies were tested on two different materials, TiAl and Ti64 in order to see the effect on two different materials.

To compare the effect of melting strategy and the material, a benchmark procedure was adopted. Replicas of the benchmark artefact have been produced using the Arcam A2X machine present in the IAM laboratory of the Polytechnic of Turin.

The dimensional and geometric measurements were carried out in the laboratory of the company ASF Metrology, using a coordinate measuring machine (CMM).

To have a systemic view of the dimensional tolerances associated with the process, the IT grade was used. While for the geometric quality the geometric tolerances were compared using the statistical tools.

The results showed that the strategy with contour leads to a significant improvement in the shape and orientation of the produced pieces. In addition, from the comparison between Ti64 and TiAl it seems that the Contour technique has a better effect on the geometric quality as the temperature of the process increases and with slower

cooling. However, the best geometric quality of the Contour comes at the cost of an incorrect dimensional quality compared to the piece produced without contour.

A possible solution to maximize the total quality of the pieces could be the use of contour by applying a scale factor in the X, Y, Z directions. In this way, in addition to having a better shape and orientation, there would be no side effect on dimensional quality.

From the studies carried out it was possible to further investigate the capabilities of this production technique with a high innovative potential, such as the Electron Beam Melting. However, the conclusions deriving from the analysis must not be considered as a final point, rather they must be a basis for future studies in order to have an ever deeper knowledge of this process, and to obtain more innovative and higher quality productions.

ACKNOWLEDGEMENTS

First of all, my gratitude go to the supervisor of this thesis, Professor Luca Iuliano, for giving me the opportunity to know and work on the innovative world of Additive Manufacturing. Also thank you for all the advice you gave me in difficult moments.

I thank the engineer Manuela Galati, co-supervisor of the thesis, for giving me considerable support in carrying out this thesis, during such a difficult period for everyone. Thank you for having believed in me and for your great help.

I thank Professor Paolo Minetola, co-supervisor of the thesis, for his precious advice and for his availability.

I sincerely thank the measurement manager Marco Ebano of ASF Metrology for welcoming me to his company, in a context where it would have been difficult to complete the thesis in time without his help.

I thank the Politecnico and all the professors over the years, not only because they made me an engineer, but also because I grew up not only professionally but also as a person with them.

I thank my family for the great support they have given me all these years, for believing in me and my choices.

Finally, I thank my friends, for the wonderful university years spent together and for the support you give me at any time.

REFERENCES

[1] J. Karlsson, A. Snis, H. Engqvist, and J. Lausmaa, “Characterization and comparison of materials produced by Electron Beam Melting (EBM) of two different Ti-6Al-4V powder fractions,” *J. Mater. Process. Technol.*, vol. 213, no. 12, pp. 2109–2118, 2013.

[2] H. Clemens and S. Mayer, “Design, processing, microstructure, properties, and applications of advanced intermetallic TiAl alloys,” *Adv. Eng. Mater.*, vol. 15, no. 4, pp. 191–215, 2013.

[3] M. Galati and L. Iuliano, “A literature review of powder-based electron beam melting focusing on numerical simulations,” *Addit. Manuf.*, vol. 19, pp. 1–20, 2018.

[4] S. Biamino *et al.*, “Electron beam melting of Ti-48Al-2Cr-2Nb alloy: Microstructure and mechanical properties investigation,” *Intermetallics*, vol. 19, no. 6, pp. 776–781, 2011.

[5] O. H. Ulf Lindhe, “Rapid Manufacturing with Electron Beam Melting (EBM) – A manufacturing revolution?,” vol. 2006, no. 2006.11.27, pp. 433–438, 2003.

[6] A. J. Nathan and A. Scobell, “How China sees America,” *Foreign Aff.*, vol. 91, no. 5, pp. 1689–1699, 2012.

[7] A. Barz, T. Buer, and H. D. Haasis, “A Study on the Effects of Additive Manufacturing on the Structure of Supply Networks,” *IFAC-PapersOnLine*, vol. 49, no. 2, pp. 72–77, 2016.

[8] Arcam, “EBM system Cobalt Chrome Alloy ASTM F 75 CoCr Alloy ASTM F75 ASTM F 75 CoCr Alloy,” *ASTM 75 CoCr Alloy*, no. noVEmBEr, p. 3, 2007.

[9] T. R. Mahale, “Electron beam melting of advanced materials and strucutres,”p.

219, 2009.

[10] S. Tammas-Williams, H. Zhao, F. Léonard, F. Derguti, I. Todd, and P. B. Prangnell, “XCT analysis of the influence of melt strategies on defect population in Ti-6Al-4V components manufactured by Selective Electron Beam Melting,” *Mater. Charact.*, vol. 102, pp. 47–61, 2015.

[11] J. Milberg and M. Sigl, “Electron beam sintering of metal powder,” *Prod. Eng.*, vol. 2, no. 2, pp. 117–122, 2008.

[12] S. M. Gaytan, L. E. Murr, F. Medina, E. Martinez, M. I. Lopez, and R. B. Wicker, “Advanced metal powder based manufacturing of complex components by electron beam melting,” *Mater. Technol.*, vol. 24, no. 3, pp. 180–190, 2009.

[13] J. Schwerdtfeger, R. F. Singer, and C. Körner, “In situ flaw detection by IR-imaging during electron beam melting,” *Rapid Prototyp. J.*, vol. 18, no. 4, pp. 259–263, 2012.

[14] Y. Chen, H. Yue, and X. Wang, “Microstructure, texture and tensile property as a function of scanning speed of Ti-47Al-2Cr-2Nb alloy fabricated by selective electron beam melting,” *Mater. Sci. Eng. A*, vol. 713, no. December 2017, pp. 195–205, 2018.

[15] C. Körner, E. Attar, and P. Heinl, “Mesoscopic simulation of selective beam melting processes,” *J. Mater. Process. Technol.*, vol. 211, no. 6, pp. 978–987, 2011.

[16] J. Zhou *et al.*, “Research on aluminum component change and phase transformation of TiAl-based alloy in electron beam selective melting process under multiple scan,” *Intermetallics*, vol. 113, no. August, p. 106575, 2019.

[17] D. D. Deligianni, N. Katsala, S. Ladas, D. Sotiropoulou, J. Amedee, and Y. F. Missirlis, “Effect of surface roughness of the titanium alloy Ti-6Al-4V on human

bone marrow cell response and on protein adsorption," *Biomaterials*, vol. 22, no. 11, pp. 1241–1251, 2001.

[18] D. L. Schmidt, "Simulation of Turbine Airfoil Surface Roughness and Associated Heat Transfer," vol. 120, no. April 1998, pp. 337–342, 2015.

[19] A. Safdar, H. Z. He, L. Y. Wei, A. Snis, and L. E. Chavez De Paz, "Effect of process parameters settings and thickness on surface roughness of EBM produced Ti-6Al-4V," *Rapid Prototyp. J.*, vol. 18, no. 5, pp. 401–408, 2012.

[20] E. C. Santos, M. Shiomi, K. Osakada, and T. Laoui, "Rapid manufacturing of metal components by laser forming," *Int. J. Mach. Tools Manuf.*, vol. 46, no. 12–13, pp. 1459–1468, 2006.

[21] S. Franchitti *et al.*, "Investigation on Electron Beam Melting: Dimensional accuracy and process repeatability," *Vacuum*, vol. 157, no. July, pp. 340–348, 2018.

[22] B. Vayre, F. Vignat, and F. Villeneuve, "Identification on some design key parameters for additive manufacturing: Application on Electron Beam Melting," *Procedia CIRP*, vol. 7, pp. 264–269, 2013.

[23] P. Minetola, L. Iuliano, and G. Marchiandi, "Benchmarking of FDM Machines through Part Quality Using IT Grades," *Procedia CIRP*, vol. 41, pp. 1027–1032, 2016.

[24] "Arcam EBM," *GE Addit.*, p. 2, 2019.

[25] "ISO 286 -Tolerance-Part-1.pdf." .

[26] Z. Quan *et al.*, "Additive manufacturing of multi-directional preforms for composites: Opportunities and challenges," *Mater. Today*, vol. 18.